The bombardment history of the Moon as recorded by ^{40}Ar-^{39}Ar chronology

V. A. FERNANDES[1,2,3*], J. FRITZ[1], B. P. WEISS[4], I. GARRICK-BETHELL[5,6],
and D. L. SHUSTER[2,3]

[1]Museum für Naturkunde, Leibniz-Institut für Evolutions- und Biodiversitätsforschung, Berlin 10115, Germany
[2]Berkeley Geochronology Centre, Berkeley, California 94709, USA
[3]Department of Earth and Planetary Science, University of California-Berkeley, Berkeley, California 94720, USA
[4]Department of Earth, Atmospheric, and Planetary Sciences, Massachusetts Institute of Technology, Cambridge,
Massachusetts 02139, USA
[5]Earth & Planetary Sciences, University of California-Santa Cruz, Santa Cruz, California 95064, USA
[6]Kyung Hee University, School of Space Research, South Korea
[*]Corresponding author. E-mail: veraafernandes@yahoo.com or vera.fernandes@mfn-berlin.de

Abstract–New petrography and ^{40}Ar-^{39}Ar ages have been obtained for 1–3 mm sized rock fragments from Apollo 16 Station 13 soil 63503 (North Ray crater ejecta) and chips from three rocks collected by Apollo 16 and Apollo 17 missions. Selection of these samples was aimed at the old ^{40}Ar-^{39}Ar ages to understand the early history of the lunar magnetic field and impact flux. Fifteen samples were studied including crustal material, polymict feldspathic fragmental breccias, and impact melts. The impact ages obtained range between approximately 3.3 and 4.3 billion years (Ga). Polymict fragmental breccia 63503,1 exhibits the lowest signs of recrystallization observed and a probable old relic age of 4.547 ± 0.027. The plateau age of 4.293 ± 0.044 Ga obtained for impact melt rock 63503,13 represents the oldest known age for such a lithology. Possibly, this age represents the minimum age for the South Pole-Aitken (SPA) Basin. In agreement with literature data, these results show that impact ages >3.9 Ga are found in lunar rocks, especially within soil 63503. Impact exhumation of deep-seated warm crustal material onto the lunar surface is considered to explain the common 4.2 Ga ages obtained for weakly shocked samples from soil 63503 and Apollo 17. This would directly imply that one or more basin-forming events occurred at that time. Some rock fragments showing none to limited petrologic features indicate thermal annealing. These rocks may have lost Ar while resident within the hot-ejecta of a large basin. Concurrent with previous studies, these results lead us to advocate for a complex impact flux in the inner solar system during the initial approximately 1.3 Ga.

INTRODUCTION

The scarred surface of the Moon has been shaped by an intense bombardment of impactors. The impact events formed a higher density of craters over the ancient lunar crust than on the maria (basaltic lava flows, often confined within the large basins) due to the younger ages of the mare flows and a lower impact flux during the past approximately 3.5 Ga. It is generally accepted that the primary lunar crust formed more than 4.4 Ga ago (Jessberger et al. 1974; Nyquist et al. 1981; Carlson and Lugmair 1988; Snyder et al. 2000; Norman et al. 2003). Thereafter, lunar stratigraphy is divided into five main systems, from oldest to youngest: pre-Nectarian (30 impact basins; a basin is a crater ≥300 km), Nectarian (12 basins), Imbrian (3 basins), Erastothenian (0 basins), and Copernican (0 basins) (Wilhelms 1987). The current estimate of 45 basins (Wilhelms 1987) is being challenged as new detailed elevation maps are available from orbiting spacecraft, with the suggestion that the lunar basin population is probably 2–3 times larger (Frey 2011). Based on sample age data, estimates of basin ages formation are probably dominated by laterally extensive basin

deposits: Nectaris (Jansen Formation), Imbrium (Fra Mauro Formation), and Orientale (Hevelius Formation). The Erastothenian and Copernican systems, in which no major basin events occurred, are identified based on crater size-frequency distribution. The largest basins in the pre-Nectarian system are South Pole Aitken (SPA), Tranquilitatis, and Fecunditatis. Basins in the Nectarian system include Nectaris, Crisium, Moscovienses, and Serenitatis (Wilhelms 1987), while the Imbrium and Orientale basins belong to the lower Imbrian system. Overall, there is considerable uncertainty regarding the absolute ages of the events that formed these basins and ejecta layers (Stöffler et al. 2006). For example, the age for Nectaris Basin lies somewhere between 4.10 and 3.92 Ga and the age of Imbrium impact event is constrained to be between 3.91 and 3.77 Ga (Stöffler et al. [2006] and references therein). Also, there is some controversy on which samples are most representative for the age determination of Crisium (3.95–3.85 Ga), Serenitatis (3.98–3.87 Ga), or Orientale (3.77–3.72 Ga). The most easily recognizable basins are thus only constrained to have formed in a period between 4.10 and 3.72 Ga (an interval of approximately 380 Ma).

An important debate in lunar science concerns the dominant age of approximately 3.9 Ga obtained using different radiometric dating techniques (i.e., Ar/Ar, Rb/Sr, and U/Pb) on samples from the lunar highlands. The observed peak of radiometric ages at approximately 3.9 Ga is commonly thought to be due to either 1) the resetting of the different radiogenic chronometers (e.g., Rb/Sr, Ar/Ar) because of a concentration of impact events around 3.9 Ga (i.e., Stöffler et al. [2006] and references therein); or 2) because all Apollo missions sampled mainly Imbrium ejecta (Baldwin 1974; Haskin et al. 1998). The approximately 3.9 Ga peak does not clearly reflect whether this age demarks the end of a declining impact flux (Hartmann 1975, 2003) since the formation of the solar system (approximately 4.57 Ga: Bouvier and Wadhwa 2010) or due to a sudden increase in the flux at this time (lunar cataclysm: Turner et al. 1973; Tera et al. 1974; Ryder 1990; Bogard 1995; Bottke et al. 2007). Alternatively, the impact flux could be characterized by sporadic increases in the flux causing spikes in the size and frequency of impacts onto the lunar surface at different times (Tera et al. 1974; Cadogan and Turner 1977; Norman 2009). This has relevance for models regarding the orbital evolution of the giant planets and the architecture of the solar system (e.g., Gomes et al. 2005; Bottke et al. 2007). Moreover, the impact history of the Earth–Moon system is directly linked to the evolution of life on Earth (e.g., Shoemaker 1983; Maher and Stevenson 1988; Nisbet and Sleep 2001; Ryder 2003), and for the robustness of crater counting statistics for the initial

1 Ga of solar system history (e.g., Hartmann and Neukum 2001).

Apollo and Luna samples potentially record the lunar impact history through both their petrographic textures and radiometric ages. In this study, the thermal history of lunar rocks is investigated by high-resolution $^{40}Ar/^{39}Ar$ step-heating ages and petrographic descriptions of shock and thermal metamorphic features of Apollo 16 and Apollo 17 samples. Petrography and argon step-heating data for fragments from soil 63503 are presented. In addition, the thermal history and argon step-heating ages are revisited for the weakly shocked FAN rock 60025, the strongly shocked norite 78235 (Wilshire 1974; Jackson et al. 1975), and the thermally annealed breccia 78155 (Bickel 1977). For these rocks (in contrast to the rake samples), chronologic data from isotopic systems with different closure temperatures are available (Schaeffer and Husain 1973, 1974; Turner and Cadogan 1975; Nyquist et al. 1981, 2008; Aeschlimann et al. 1982; Carlson and Lugmair 1988; Premo and Tatsumoto 1991; Borg et al. 2011).

To acquire a more comprehensive view of the impact history of the Earth–Moon system, these data are integrated with isotopic ages reported by other groups (Kirsten et al. 1973; Schaeffer and Husain 1973, 1974; Kirsten and Horn 1974; Cadogan and Turner 1976, 1977; Schaeffer and Schaeffer 1977; Maurer et al. 1978; McGee et al. 1978; Staudacher et al. 1978; Dalrymple and Ryder 1996; Culler et al. 2000; Levine et al. 2005; Barra et al. 2006; Norman et al. 2006, 2007; Zellner et al. 2006; Hudgins et al. 2008).

APOLLO 16 AND APOLLO 17 LANDING SITES OVERVIEW

Apollo 16 landed on the relatively smooth Cayley Plains between the bright North and South Ray craters. The smooth and low-lying Cayley Formation extends to the west and north. To the east and south is the hilly terrain of the Descartes Mountains Formation. Regionally, surface materials at the Apollo 16 landing site are dominated by the 70–220 m thick Cayley Formation (Hodges et al. 1973) lying on top of the Descartes Formation (approximately 1 km thick; Milton 1968). Apollo 16 samples are commonly divided into a KREEP-free "Old Eastern Highland Rock Suite" and a KREEP-bearing "Young Western Highland Rock Suite" (Stöffler et al. 1985; Korotev 1994; KREEP: K = potassium, REE = rare earth elements, and P = phosphorus; and also enriched in U and Th-elements). The Descartes Formation is interpreted as being either 1) ejecta from the Nectaris Basin probably modified by the Imbrium impact (Stöffler et al. 1985); or 2) emplaced or reworked Imbrium ejecta (Hodges

et al. 1973; Ulrich 1973; Norman et al. 2010). The Cayley Formation is generally interpreted as a continuous deposit from the Imbrium Basin that may have been modified by the event that formed the Orientale Basin (Hörz et al. 1981; Spudis 1984; Wilhelms 1987). The soil fragments used in this study were collected at Station 13 and were described by Korotev (1997) as being ejecta from the North Ray crater (1000 m diameter and 230 m depth; Wilhelms 1987). Beside Apollo 16 station 11 (Smoky Montain) the North Ray crater ejecta is considered to be the best source for samples from the Descartes Formation (Stöffler et al. 1985).

The Apollo 17 landing site is located in a deep, narrow valley called Taurus-Littrow on the eastern rim of Mare Serenitatis. The landing site is in a dark deposit between massifs of the southwestern Montes Taurus and south of the dark haloed crater Littrow. This crater has been interpreted as a cinder cone probably formed by explosive volcanic activity (e.g., Wilhelms 1987). The valley floor is essentially flat with only a gentle incline. It is located about 750 km east of the Apollo 15 landing site and about the same distance north of the Apollo 11 landing site. Due to its old appearance, Serenitatis Basin was suggested by Wilhelms and McCauley (1971) and Head (1974) to be pre-Imbrium in age. The highlands near the eastern Mare Serenitatis appeared to have Imbrium influence in the form of radial striations and blanketing deposits. However, ancient rock was probably exposed at relatively sharp massifs of pre-Imbrium Serenitatis Basin rim (Wilhelms 1992). From the South Massif, there is a continuous, relatively younger, bright-mantle initially thought to represent ancient rock (Wilhelms 1992), and thus, it would probably provide some understanding on the basin-forming processes. Similarly, distinct units of tightly packed domical features termed Sculptured Hills were thought to provide information on basin formation processes. The morphology of the Sculptured Hills appears similar to the knobby ejecta of the Orientale and Imbrium basins (Montes Roock and Alpes, respectively). The relative age of the Serenitatis Basin is based on the distribution and stratigraphic relations of the Sculptured Hills. Apollo 17 Station 8 was chosen with the aim to obtain material from the Sculptured Hills, which was interpreted as an ejecta facies from the Serenitatis Basin (Wolfe et al. 1981; Head 1974, 1979). However, ages obtained from highland samples brought by the Apollo 17 mission, and identified as originating from the Serenitatis Basin, suggested this basin to be slightly older (approximately 3.87 Ga) than Imbrium (approximately 3.85 Ga) (Stöffler et al. 2006). Spudis and Ryder (1981) suggested that the Sculptured Hills are instead deposited over large crater rims that are superposed on the Serenitatis rim and their radial lineation suggests a relation to Imbrium Basin ejecta (Spudis and Ryder 1981). Spudis et al. (2011), using recent high-resolution images from lunar reconnaissance orbiter camera (LROC) wide angle camera (WAC), renew the suggestion that Sculptured Hills are a facies of Imbrium ejecta. Moreover, Spudis et al. (2011), Haskin (1998), and Haskin et al. (1998) suggested that Imbrium ejecta material overlies a multitude of large post-Serenitatis impact craters. By implication, most material having a KREEP signature was suggested by Haskin et al. (1998) to be derived from the Imbrium Basin.

SAMPLE SELECTION AND METHODS

The Apollo 16 and Apollo 17 rocks and 1–3 mm soil fragments studied here were originally obtained from NASA for paleomagnetic analyses based on previous studies suggesting very ancient $^{40}Ar/^{39}Ar$ ages (Kirsten et al. 1973; Kirsten and Horn 1974; Huneke and Wasserburg 1975; Husain and Schaeffer 1975; Turner and Cadogan 1975; Maurer et al. 1978; Nyquist et al. 1981; Aeschlimann et al. 1982). Soil 63503 fragments were handpicked from the parent splits 63503,77 and 63503,79 with the main focus on selecting what appeared to be anorthositic breccias. From split 63503,77, 10 fragments were chosen and given the numbers 1–10 (i.e., 63503,77,1, hereon labeled 63503,1). Similarly, from split 63503,79, 14 fragments were chosen and given numbers from 11 to 24 (i.e., 63503,79,11, hereon labeled 63503,11). One fragment was obtained from split 78235,139 (hereon labeled 78235), another from 78155,9,154 (hereon labeled 78155), and one fragment from split 60025,845 (hereon labeled 60025).

Each sample was chipped in a class 10,000 clean room into two fractions, with one fraction analyzed with scanning electron microscopy (SEM), electron microprobe analyses (EMPA), Raman spectroscopy, and transmitted light microscopy and the second fraction used for $^{40}Ar/^{39}Ar$ age determination. Compositional and backscattered scanning electron (BSE) microscopy analyses were obtained using the University of California at Berkeley five-spectrometer CAMECA SX50 electron microprobe with online data reduction. A cup current of 15–20 nA with an acceleration potential of 15 keV, and an electron beam diameter of <2 μm was used for individual mineral analyses to minimize loss of sodium during the measurements. Peak counting time was 30 s for most elements with the exception of Na with counting time of 20 s and Mn of 40 s. The background was evaluated for 15 s on either side of the peak. BSE images were

acquired for general characterization of these samples using the same instrument. After removing the carbon-coat from the thin sections, micro-Raman spectroscopy was carried out using a notch filter based confocal Dilor LabRam with a HeNe laser of 632 nm wavelength at the Museum für Naturkunde-Berlin, to obtain crystallographic information of the analyzed minerals. $^{40}Ar/^{39}Ar$ step-heating measurements were carried out at the Berkeley Geochronology Center. Prior to step-heating analyses, the fraction of the Apollo 16 and Apollo 17 samples separated for age determination were irradiated for 100 h in the Cd-shielded CLICIT facility (to minimize undesirable isotopic interference reactions) of the TRIGA reactor at Oregon State University, USA. Bulk samples and the neutron fluence monitor PP-20 hornblende (the same as Hb3gr: Turner et al. 1971; Jourdan and Renne 2007; Schwarz and Trieloff 2007) were loaded into pits within two aluminium disks. Samples are loaded in pits carved into Al-disks, and 2–3 age-monitors are put in pits between the samples. An average J-value is calculated per disk, and used for the samples in that disk. All errors reported are shown at 1σ level. The J-values for the two irradiation disks are 0.02647 ± 0.00059 and 0.02645 ± 0.00021 (see Appendix S3 for data tables and respective J-value used per sample) and were calculated relative to an age of Hb3gr = 1072 ± 11 Ma (Turner et al. 1971) and using the decay constants of Steiger and Jäger (1977). The uncertainty related to the determination of each J-value (0.8–2.0%; 1σ) is included in the age calculation. The propagation of the J-value error causes a very small change in the age error: a 20 times increase in the error in the J-value corresponds to a 0.45% increase in the calculated age error. The corrections to account for the decay of ^{37}Ar, during and after irradiation until analyses were performed, were done according the generalized equation by Wijbrans (1985) and after Brereton (1972) and Dalrymple et al. (1981). The correction factors and respective errors for interfering isotopes correspond to the weighted mean of 10 years of measurements of K–Fe and $CaSi_2$ glasses and CaF_2 fluorite in the TRIGA reactor: $(^{39}Ar/^{37}Ar)_{Ca}$ = $(6.95 \pm 0.09) \times 10^{-4}$, $(^{36}Ar/^{37}Ar)_{Ca} = (2.65 \pm 0.02) \times 10^{-4}$, $(^{40}Ar/^{39}Ar)_K = (7.30 \pm 0.902) \times 10^{-4}$, and $(^{38}Ar/^{39}Ar)_K = (12.20 \pm 0.03) \times 10^{-3}$. Before argon was measured, each bulk soil fragment was inserted in a platinum-iridium foil packet to couple with a 30 W diode laser ($\lambda = 810$ nm) and to improve temperature control (Cassata et al. 2009; Shuster et al. 2010). Up to 32 heating steps were performed to degas each sample using pyrometer feedback control. The gas was purified in a stainless steel extraction line using two Zr-Al C-50 getters and a cryogenic condensation trap. Argon isotopes were measured in static mode using a MAP 215-50 mass spectrometer with a Balzers electron multiplier, using 10 cycles of peak-hopping. A detailed description of the mass spectrometer and extraction line is given by Renne et al. (1998). Blank measurements were generally obtained after every three sample runs, and typical blanks in nA are at 1σ: $^{40}Ar = 4.85 \pm 0.02 \times 10^{-2}$, $^{39}Ar = 0.70 \pm 0.20 \times 10^{-4}$, $^{38}Ar = 6.50 \pm 0.70 \times 10^{-5}$, $^{37}Ar = 3.13 \pm 0.10 \times 10^{-4}$, and $^{36}Ar = 2.65 \pm 0.07 \times 10^{-4}$. Mass discrimination was monitored several times a day by analysis of air aliquots from an online pipette system and provided a mean value of 1.008 ± 0.0018 per atomic mass unit. Ar isotopic data were corrected for blank, mass discrimination, interference, and radioactive decay. In several cases, the $^{40}Ar/^{39}Ar$ analyses were replicated using multiple sample aliquots. The sample weight varied from 0.32 to 1.24 mg. Further details for data reduction procedures are given in Burgess and Turner (1998), Renne et al. (1998), Fernandes et al. (2000, 2003), and Fernandes and Burgess (2005). All uncertainties shown in the figures are at the 1σ level.

PETROGRAPHY AND CHEMISTRY OF THE APOLLO 16 AND APOLLO 17 SAMPLES

A total of 15 different samples from Apollo 16 (60025 and 12 fragments from soil 63503) and Apollo 17 (78155, 78235) were investigated. Sample 60025 was collected near where the lunar module (LM) landed, and soil 63503 was collected at Station 13 located on the North Ray Crater ejecta, approximately 2 km north of the LM. The Apollo 17 samples were collected at Station 8 situated on the foothills of the Sculptured Hills, approximately 4 km E of the LM and approximately 2 km NE of Camelot and Horatio craters.

Shock-pressure and -temperature determinations will be provided for the relatively large (>200 g), and well-studied rocks (e.g., Jackson et al. 1975; Bickel 1977; James et al. 1991) 78155, 78235, and 60025. The petrology and chemical composition of the 12 fragments of mm size from the rake soil sample 63503 were not previously investigated. Other fragments from this rake sample were previously characterized by Maurer et al. (1978) and James (1981). The petrographic, geochemical, and shock metamorphic results and the type of investigations applied are summarized in Tables 1 and 2 and Fig. 1. BSE images of each sample are shown in Figs. 2–6. Additional information on the studied samples, including optical micrographs in transmitted and polarized light are provided in Figs. S1–S5 in Appendix S1. Petrographic study of the samples enabled them to be categorized as (Tables 1–3): (1) fragments from crustal rocks (78155, 78235,139,

Table 1. Chemical composition and modal abundances.

Sample	Analytics	Chemical composition			Modal abundance in %vol			
		Pl	Ol	Px	Pl	Ol	Px	tr
Apollo 16								
Crustal rock								
60025,1	1–3	An_{96-98}	None	$En_{67-56}Fs_{30-41}$ Wo_{2-10} $En_{35-38}Fs_{13-28}$ Wo_{21-49}	>98	Non	<2, incl.	
63503,11	1–4	An_{96-98}	None	$En_{51-58}Fs_{35-43}Wo_{5-12}$ $En_{35-43}Fs_{12-20}Wo_{40-45}$	~95		~5	Sp
63503,15	1–4	An_{95-97}	None	Px	~99		<1 in matrix	
63503,20	1–4	An_{95-97}	None	$En_{56-64}Fs_{33-41}Wo_{2-3}$ $En_{38-42}Fs_{13-19}Wo_{40-45}$	>90	Non	<10 opx grains + cpx incl	
63503,21	1–4	An_{97-98}	Fo_{43-44}	Cpx	>90	<5	<2 incl	
63503,16	1–4	An_{96-98}	Fo_{48-50}	Cpx	>90	<5	<5	Tr
63503,14	1–4	An_{96}		Opx			<1	
63503,17	1–4	An_{96-98}	Fo_{79-80}	$En_{80}Fs_{17}Wo_3$	~80	~20	<1	Cr
Breccia								
63503,1	1–2; 4	An_{92-97}			~90	~1	~8	Il, Cr FeNi
63503,3	1–2; 4	An_{95-98}	Fo_{61-62}	$En_{56-67}Fs_{30-34}Wo_{3-10}$ $En_{37-49}Fs_{16-28}Wo_{21-50}$	~90	~2	~8	Cr, FeNi
63503,4	1–2; 4	An_{97-98}	None	$En_{60-56}Fs_{41-38}$ Wo_{2-4} $En_{38-41}Fs_{14-18}$ Wo_{44-45}	~95		~5	Il
Impact melt								
63503,9	1–2; 4	An_{83-97}	None	$En_{43-48}Fs_{19-31}$ Wo_{37-21}	~95		~4	FeNi
63503,13	1–2; 4	An_{93-96}	Fo_{61-63}	$En_{63-66}Fs_{23-30}Wo_{3-11}$ $En_{51-57}Fs_{19-23}Wo_{22-29}$	~95	~1	~4	
Apollo 17								
Crustal rock								
78155	1–3	An_{94-97}	Fo_{65}	$En_{60-63}Fs_{26-30}Wo_{8-13}$ $En_{46}Fs_{17}Wo_{36}$	~75	~10	~15	Cr, Il
78235	1–3	An_{93-94}	None	$En_{77-78}Fs_{19-20}$ Wo_{2-3}	~50		~50	Cr

Analytics: 1 = scanning electron microscopy, 2 = Electron microprobe analyses, 3 = Raman spectroscopy; 4 = Optical mircroscopy; note that thick sections were studied by optical microscopy, thus interference colors are of higher order compared with thin sections of 30 µm sample depth. Modal abundance derived by BSE image analyses.

Pl = plagioclase; Ol = olivine; Px = pyroxene; Cpx or Opx = clinopyroxen or orthopyroxene identified by Raman; spectroscopy; incl = mineral occurs as few micron-sized inclusions in plagioclase. Tr = accessory mineral, Cr = chromite, Il = ilmenite. Sp = Ti and Cr rich spinel. Tr = troilite; FeNi = µm-sized iron-nickel phases.

60025,1, and the 1–3 mm sized soil fragments 63503,11, -,14, -,15, -,16, -,17, -,20, and -,21); (2) polymict fragmental breccias (63503-,1, -,3, and -,4); and (3) impact melt rocks 63503,9 and -,13. With the exception of the Apollo 17 rocks and the soil fragment 63503,17, which are akin to the Mg-suite, all other samples are ferroan anorthosite (FAN) rocks (Fig. 1).

Apollo 17 Samples

Samples 78155 and 78235 (Figs. 2a and 2b) are shocked crustal Mg-suite rocks (Bickel 1977; Wilshire 1974; Jackson et al. 1975). Sample 78155 (Fig. 2a) is a thermally annealed polymict breccia of anorthositic norite composition (Bickel 1977). Although no thin sections for optical microscopy were available, Raman spectroscopy (see Fritz et al. [2005a] for procedure details) revealed that its plagioclase is crystalline,

indicating maximum shock pressures of 20–24 GPa (Stöffler et al. 2006; Fernandes et al. 2010).

Sample 78235 (Fig. 2b) is a heavily shocked, coarse-grained norite cumulate akin to Mg-suite rocks (Wilshire 1974) and represents the only large, unbrecciated norite collected on the lunar surface (Jackson et al. 1975). Our Raman spectroscopic investigations revealed that plagioclase in 78235 is almost completely transformed into maskelynite, indicating peak shock pressures approximately 24 GPa (Stöffler et al. 2006; Fernandes et al. 2010). Mafic minerals are dominantly represented by low-Ca pyroxene ($En_{78}Fs_{19}Wo_3$). Earlier Sm-Nd age determinations suggest that sample 78235 crystallized at 4.43 ± 0.05 Ga (Nyquist et al. 1981; and by U-Pb, Premo and Tatsumoto 1991). However, more recent Sm-Nd work by Nyquist et al. (2008) suggests a younger crystallization age of 4.320 ± 0.087 Ga for sample 78235. $^{40}Ar/^{39}Ar$ ages of 4.22 ± 0.04 Ga are

Table 2. Petrography and shock-metamorphism.

		Shock features					Petrology	
Sample	Rock type	Pl	Ol	Px	GPa	Shock stage	Deformation	Annealing
Apollo 16								
Crustal rock								
60025,1	Anorth.					Ia–Ib	Cataclasis	n.d.
63503,11	Anorth.	A				Ia–Ib	Granular bands	No – weak
63503,15	Anorth.	A			10–25	Ia-Ib	Cataclasis	No – weak
63503,20	Anorth.	A		a	10–25	Ia-Ib	Cataclasis	No – weak
63503,21	Anorth.	A	a		10–25	Ia-Ib	Cataclasis	Partly
63503,16	Anorth.	A	a		10–25	Ia-Ib	Cataclasis	Strong
63503,14	Anorth.	No	No	No	No	0	No	Partly
63503,17	Anorth. Troc.	No	No	No	No	0	No	No
Breccia								
63503,1	PB	No	No	No	No	0–Ib	Breccia	n.d.
63503,3	PB	No	No	No	No	0	Breccia	Partly
63503,4	PB	No	No	No	No	0	Breccia	Strong
Impact melt								
63503,9	Anorth.	No	No	No	No	0	No	–
63503,13	Noritic Anorth.	No	No	No	No	0	No	–
Apollo 17								
Crustal rock								
78155	Noritic Anorth.	Pl	n.d.	n.d.	<25	0–Ib	Breccia	Strong[a]
78235	Norite	B		n.d.	25–30	2a	No	n.d.

[a]Bickel (1977).

Anorth. = anorhtosite; Anorth. Troc. = anorhtositic troctolite PB = polymict breccia: GB = granulitic breccia; Shock stages after Stöffler and Grieve (2007), using the granitic-feldspathoid scheme for anothosites and the scheme for basaltic-gabbroic rocks for the more mafic norite and troctilite. Pl = crystalline plagioclase determined by Raman spectroscopy; a = weak and A = strong undulatory extinction. B = partly crystalline plagioclase and partly maskelynite as identified by Raman spectroscopy. n.d. = not detected.
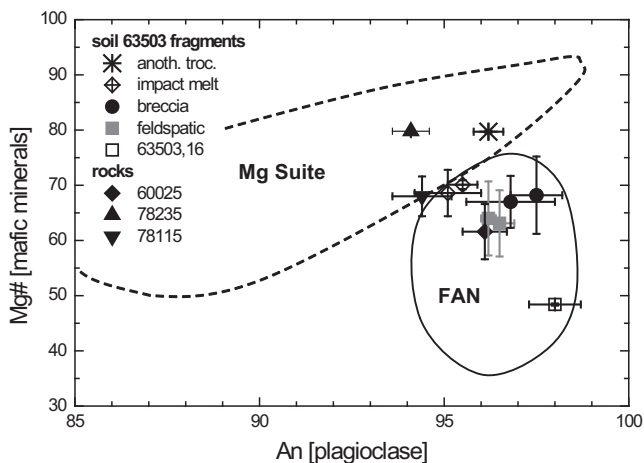

Fig. 1. Average values and standard deviations of the magnesium numbers (Mg#) of mafic minerals (ol + px) and anorthite content (An) of plagioclase for the individual rock and rake samples. Chemical composition of the individual minerals is determined by EMPA analyses and tabulated in the Appendix S3. The field for the ferroan anorthosites (FAN suite) and the magnesium suite rocks (Mg suite) is adopted from Wieczorek et al. (2006).

thought to represent impact-related disturbances (Turner and Cadogan 1975). Jackson et al. (1975) suggested that the rock actually underwent one or two disturbance events at 4.11 ± 0.02 Ga (obtained by $^{40}Ar/^{39}Ar$: Aeschlimann et al. 1982) and/or at 4.27 ± 0.02 Ga ($^{40}Ar/^{39}Ar$: Turner and Cadogan 1975; Nyquist et al. 1981).

Apollo 16 Samples

Sample 60025

Sample 60025 (Fig. 3a) is a cataclastic FAN breccia containing up to mm-sized-plagioclase fragments ($An_{96–98}$) hosting μm-sized pyroxene inclusions (Hodges and Kushiro 1973; Walker et al. 1973; Dixon and Papike 1975; Ryder 1982; James et al. 1991). No thin section for optical microscopy was available, but Raman spectroscopy indicates that all plagioclase is crystalline. Sample 60025 contains both high-Ca ($En_{36}Fs_{20}Wo_{44}$) and low-Ca ($En_{54}Fs_{44}Wo_2$) pyroxene. Previously, an Sm-Nd crystallization age of 4.44 ± 0.02 Ga (Carlson and Lugmair 1988) and an older Pb-Pb crystallization age of 4.520 ± 0.007 Ga (Hanan and Tilton 1987) were reported. Schaeffer and Husain (1973) report a ^{40}Ar-^{39}Ar shock age of 4.19 ± 0.02 Ga. More recently, Borg et al. (2011) reported a younger age of 4.360 ± 0.003 Ga obtained by using a combination of Sm/Nd and Pb/Pb isotopic data.
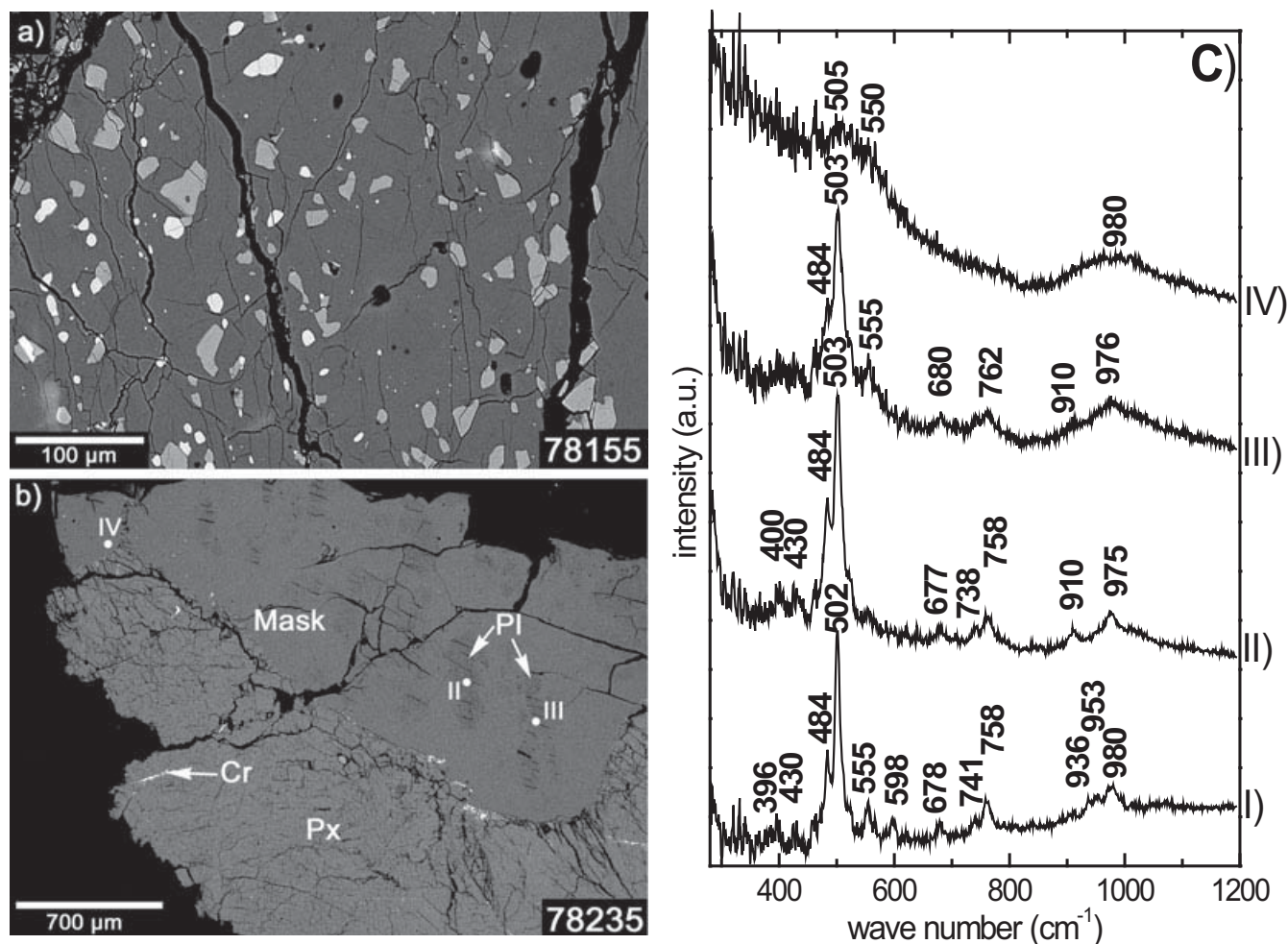
Fig. 2. Backscattered electron images (BSE) of Apollo 17 rocks a) sample 78155, a thermally annealed polymict breccia of anorthositic norite. b) BSE image of sample 78235, a heavily shocked norite cumulate with plagioclase partly shocked to maskelynite. Points I–IV show where Raman spectra were obtained. c) Raman spectra of plagioclase and maskelynite observed in sample 78235: I) spectra of unshocked plagioclase with An_{94} from troctilite 63503,17; II–IV). Crystallinity of the plagioclase decreases from I to IV with IV being indicative of complete maskelynite conversion of plagioclase. Mask = maskelynite, Pl = plagioclase, Cr = chromite, and Px = pyroxene.

Fragments from the Apollo 16, 63503 Soil

The 1–3 mm rake fragments from soil sample 63503 range from single mineral phases (e.g., plagioclase, pyroxene, olivine, and ilmenite) to lithic clasts (e.g., anorthosite, impact melt, and norite).

Crustal rocks. The anorthosites 63503,11, 63503,15, 63503,16, 63503,20, 63503,21 (Figs. 3b–f) are composed dominantly of large anorthite crystals and smaller interstitial grains of pyroxene with accessory olivine. These FAN rocks show a relict coarse-grained texture that was deformed by cataclasis and subsequent thermal annealing in a few samples (Table 2). In general, the components in the fragmental breccias are angular in shape. Using transmitted light microscopy, the finely brecciated regions appear brownish while the larger plagioclase fragments appear transparent. Most plagioclase displays strong undulatory extinction and no maskelynite is observed. We could not discern whether samples 63503,11, -,15, and -,20 were affected by weak recrystallization or if they lack any recrystallization features (Table 2) because the available thick sections are thicker than the components comprising their finely cataclastized zones. However, cataclastic anorthosites lacking recrystallization features are thought to be very rare in Apollo 16 samples (Stöffler et al. 1985).

Sample 63503,11 (Figs. 3b, S1, and S2a) almost completely consists of a single plagioclase grain cross-cut by granular bands composed dominantly of plagioclase and occasionally by pyroxene fragments. A 100 μm-diameter pyroxene grain (Figs. 3b and S1)
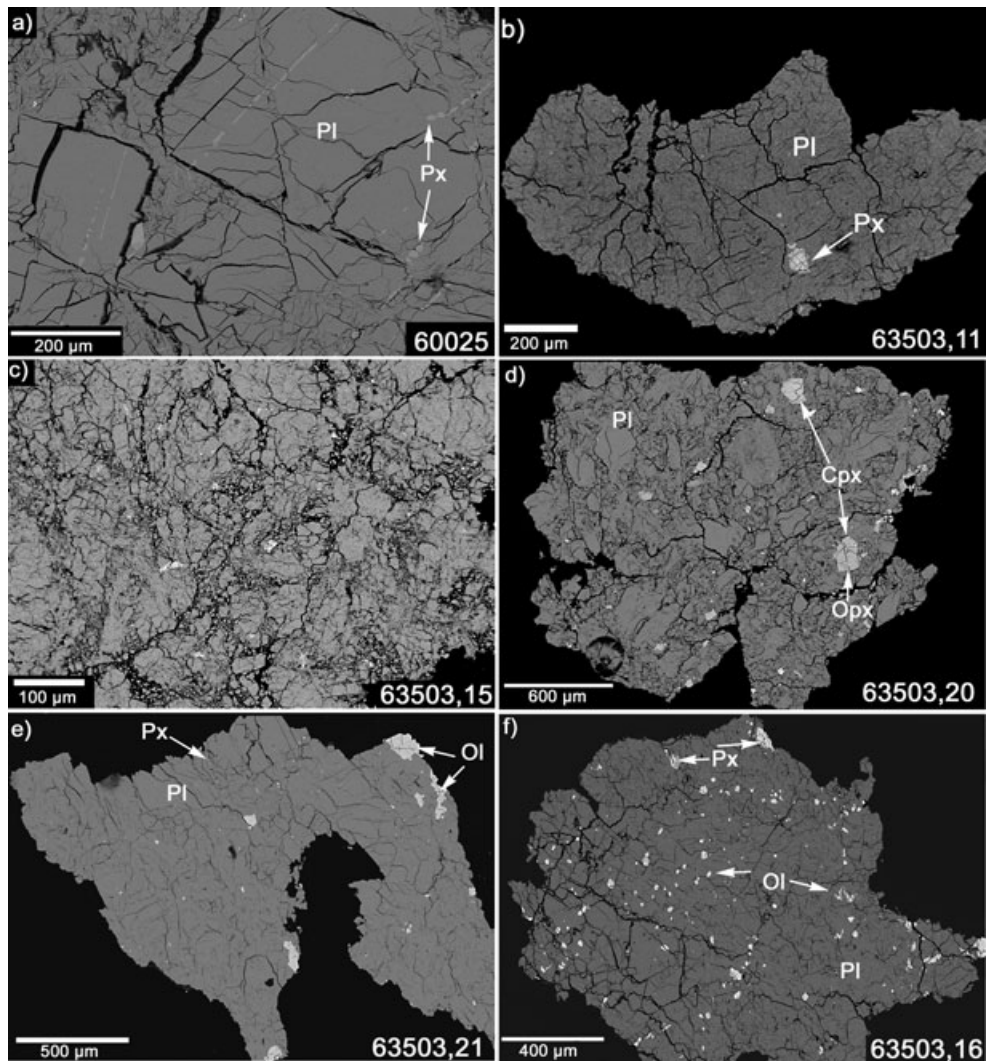
Fig. 3. BSE images of anorthosites: a) cataclastically deformed anorthosite composed of heavily fractured plagioclase with inclusions of pyroxene; b) single plagioclase grain cross-cut by granular bands; c) anorthositic breccias with traces of pyroxene in the catalastic matrix; d) anorthositic breccia with some CPx and OPx fragments; e–f) cataclastic anorthosite with minor olivine and pyroxene. Sample number is denoted in the lower right of the image. Mask = maskelynite; Pl = plagioclase; Px = pyroxene. OPx = orthopyroxene, CPx = clinopyroxene, and Ol = olivine.

contains 2 μm diameter orthopyroxene and approximately 5 μm diameter clinopyroxene exsolution lamellae with submicron sized Ti- and Cr-rich spinel inclusions in the clinopyroxene region (phase identification by Raman spectroscopy; see Fig. S1b).

Samples 63503,15 (Figs. 3c and S2b) and -,20 (Figs. 3d and S2c) are monomict anorthositic breccias with randomly oriented plagioclase fragments set in a cataclastic matrix. No signs of recrystallization were observed. In both samples, plagioclase ($An_{94–97}$) displays strong undulatory extinction and pyroxene displays weak undulatory extinction, indicating peak shock pressures of 5–20 GPa. In sample 63503,20, a 300 μm diameter plagioclase grain appears unshocked (S1c), possibly indicating that a brecciation event was

the last shock event (>5 GPa) recorded in this sample. Fragment 63503,20 shows two compositionally different pyroxenes (Fig. 3d), where orthopyroxene ($En_{61–65}Fs_{33–37}Wo_2$) is the host of small clinopyroxene ($En_{42}Fs_{13}Wo_{45}$) inclusions. In sample 63503,15 (Fig. 3c), pyroxene is only present as small fragments in the matrix and not as inclusions within the large plagioclase fragments.

Sample 63503,21 (Figs. 3e, S2e, and S2f) is dominated by anorthite ($An_{97–98}$) with minor olivine ($Fo_{43–44}$). Pyroxene occurs as inclusions in mm-sized plagioclase grains. The cataclastic anorthosite consists of a 500 μm diameter plagioclase adjacent to a brecciated zone of randomly oriented angular plagioclase fragments. One region of the brecciated zone displays a granoblastic texture in which some fragments
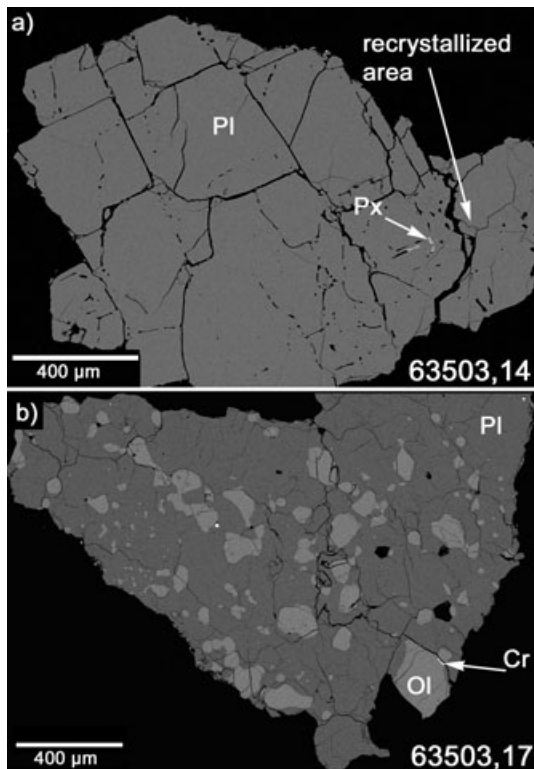
Fig. 4. BSE images of igneous rocks fragments: a) anorthosite composed of single plagioclase grain and an attached zone of recrystallised plagioclase (lower right); b) troctlite with plagioclase and olivine showing a magmatic texture. Pl = plagioclase, Px = pyroxene, Cr = chromite, and Ol = olivine.

have 120° grain boundaries (Fig. S2f). This indicates a higher degree of thermal annealing (e.g., >500 °C Kruhl [2001] and references therein) compared with the previously described anorthosites.

Sample 63503,16 (Figs. 3f and S2d) is a granoblastic to granulitic breccia. This olivine-noritic anorthosite is composed of large plagioclase fragments hosting small inclusions of clinopyroxene. Small mafic minerals such as clinopyroxene, olivine, and rarely troilite grains are also present in the feldspathic matrix. The granoblastic texture indicates a high degree of thermal annealing and recrystallization. In addition, both plagioclase (An_{96-98}) and olivine (Fo_{48-50}) crystals are fractured and plagioclase displays strong undulatory extinction, indicating peak shock pressures of approximately 10–20 GPa.

In contrast to the cataclastic anorthosites, samples 63503,14 and -,17 (Figs. 4a and 4b, S3a, and S3b) represent mechanically undeformed crustal rocks. Sample 63503,14 (Figs. 4a and S3a) is an anorthosite consisting of a chemically zoned, 800 μm diameter plagioclase grain adjacent to a granoblastic textured region containing 50–100 μm diameter plagioclase crystals with well-developed 120° grain boundaries (upper left side

of Fig. S3a). The chemically similar crystals developed different textures in the two regions, thus providing evidence for a secondary thermal event that resulted in either crystallization or recrystallization of the smaller plagioclase grains. No shock features are observed in either of the texturally different plagioclase crystals, indicating peak shock pressures <5 GPa. Sample 63503,17 (Figs. 4b and S3b) is an anorthositic troctolite composed of calcium-rich plagioclase (An_{96-98}) and magnesium-rich olivine (Fo_{79-80}) with traces of pyroxene and chromite. Olivine grains range in diameter from 10 to 400 μm and have rare orthopyroxene inclusions ($En_{80}Fs_{17}Wo_3$). Micrometer-sized clinopyroxene inclusions in plagioclase were identified by Raman spectroscopy. Both olivine and plagioclase crystals have well-developed 120° grain boundaries (S3b). The equilibrium texture indicates cooling of an igneous rock in a plutonic environment or a larger impact melt pool. Using the optical microscope with crossed polarizers, all minerals display sharp extinction and no signs of shock metamorphic overprint are observed, indicating shock pressures <5 GPa.

Polymict feldspathic fragmental breccias. The three polymict feldspathic fragmental breccias 63503,1, 63503,3, and 63503,4 (Figs. 5a–c and S4a–d) contain fragments of individual minerals (e.g., olivine, pyroxene, plagioclase, chromite) and lithic clasts. The individual mineral and lithic fragments range in diameter from approximately 2 to 30 μm and 200 to 500 μm, respectively. The majority of the lithic clasts are partly to totally metamorphosed primary rocks or even breccias, and impact melt clasts. Some impact melt clasts in samples 63503,1 and 63503,3 contain μm-sized FeNi particles (Figs. 5a and 5b). The degree of thermal annealing increases from fragment 63503,1 to 63503,4 (Figs. 5a, 5 c, S4a, and S4b). Evidence for later thermal annealing was not observed in the lithic breccia 63503,1, which has a matrix consisting mainly of mineral clasts. The lithic breccia 63503,3 (Figs. 5b, S4c, and S4d) contains crystallized (devitrified) impact melt clasts and some regions of the breccia are recrystallized in situ. The granulitic texture of breccia 63503,4 documents strong thermal annealing and complete recrystallization. The relic olivine and pyroxene in this sample developed reaction rims with the neighbouring plagioclase crystals and melt.

Impact melts. Two very distinct impact melt rocks were identified amongst the particles analyzed, 63503,9 and 63503,13 (Figs. 6a, 6b, and S5a–c). The intergranular impact melt rock 63503,9 (Figs. 6a and S5c) is composed of angular to subrounded plagioclase fragments (An_{94-97}) surrounded by interstitial and unequilibrated quenched pyroxenes ($En_{43-48}Fs_{19-31}Wo_{37-21}$) and a myriad of pores. The interstitial regions in 63503,9 host a large number of μm-sized FeNi
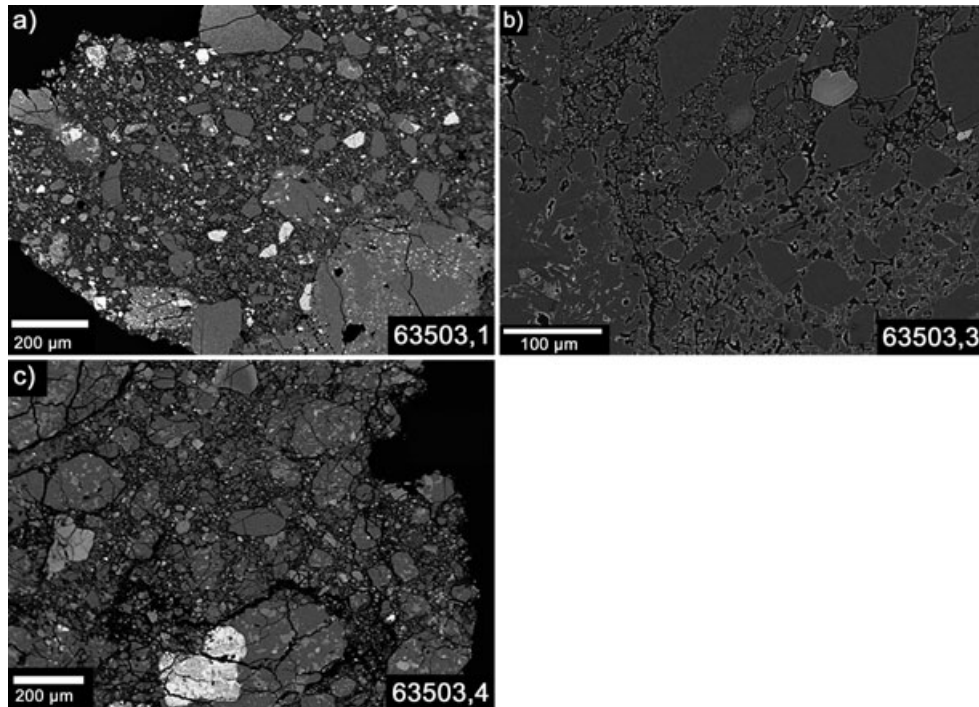
Fig. 5. BSE images of a–c) feldspathic breccia consisting of mineral, lithic, and impact melt clasts. The sample number is denoted in the lower right of the image. Pl = plagioclase, Ol = olivine, Cr = chromite, and Px = pyroxene.
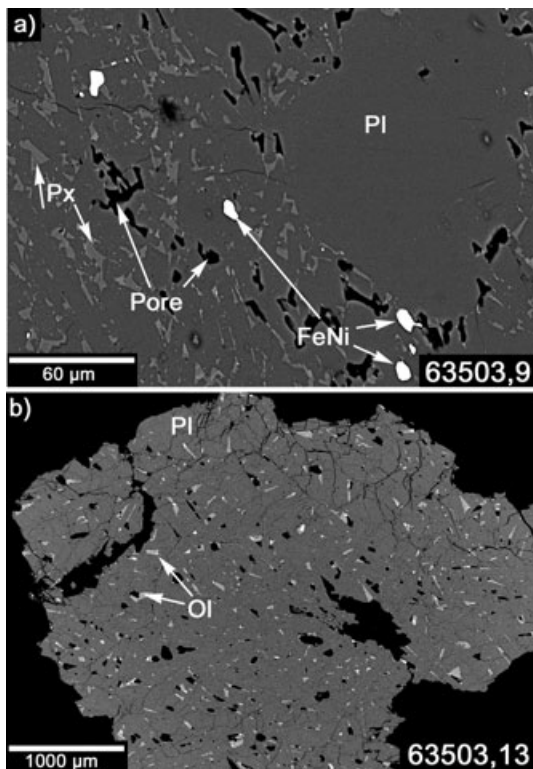

Fig. 6. BSE images of impact melt rocks: a) granulitic impact melt rock with μm-sized FeNi particles; b) impact melt rock composed of plagioclase lath with interstitial olivine and pyroxene. Pl = plagioclase and Px = pyroxene.

particles (Ni up to 30 wt%), but no sulfur-rich particles (i.e., troilite). The intersertal impact melt rock 63503,13 (Fig. 6b, S5a, and S5b) is composed of plagioclase laths (An_{93-96}) radially emerging from different centers and cross-cutting each other. Olivine (Fo_{61-63}) and orthopyroxene ($Opx = En_{63-66}Fs_{23-30}Wo_{3-11}$ and $Cpx = En_{51-57}Fs_{19-23}Wo_{22-29}$) occur interstitially. Vesicles were observed in a few regions of the quickly quenched melt (S5b). The texture of the intersertal melt rock indicates cooling in a melt sheet thicker than 5 m to allow formation of plagioclase crystals (see Deutsch and Stöffler [1987] and references therein). This indicates a later emplacement to the Apollo 16 site. In contrast, the quickly quenched intergranular impact melt rock could be directly transported to the Apollo 16 site.

Petrological Constraints on the Thermal History

In the 15 lunar samples studied, we have documented a range of shock pressures from unshocked (<5 GPa for 63053,13, 63503,14, and 63503,17) to moderately shocked (20–24 GPa, for 60025 and 78235). As a group, the FAN suite rocks from 63503 soil are weakly shocked (5–20 GPa) with plagioclase displaying strong undulatory extinction. Generally, nonporous igneous rocks, in which plagioclase was not transformed into maskelynite, experienced a postshock temperature increase of <100–200 °C (i.e., Artemieva and Ivanov
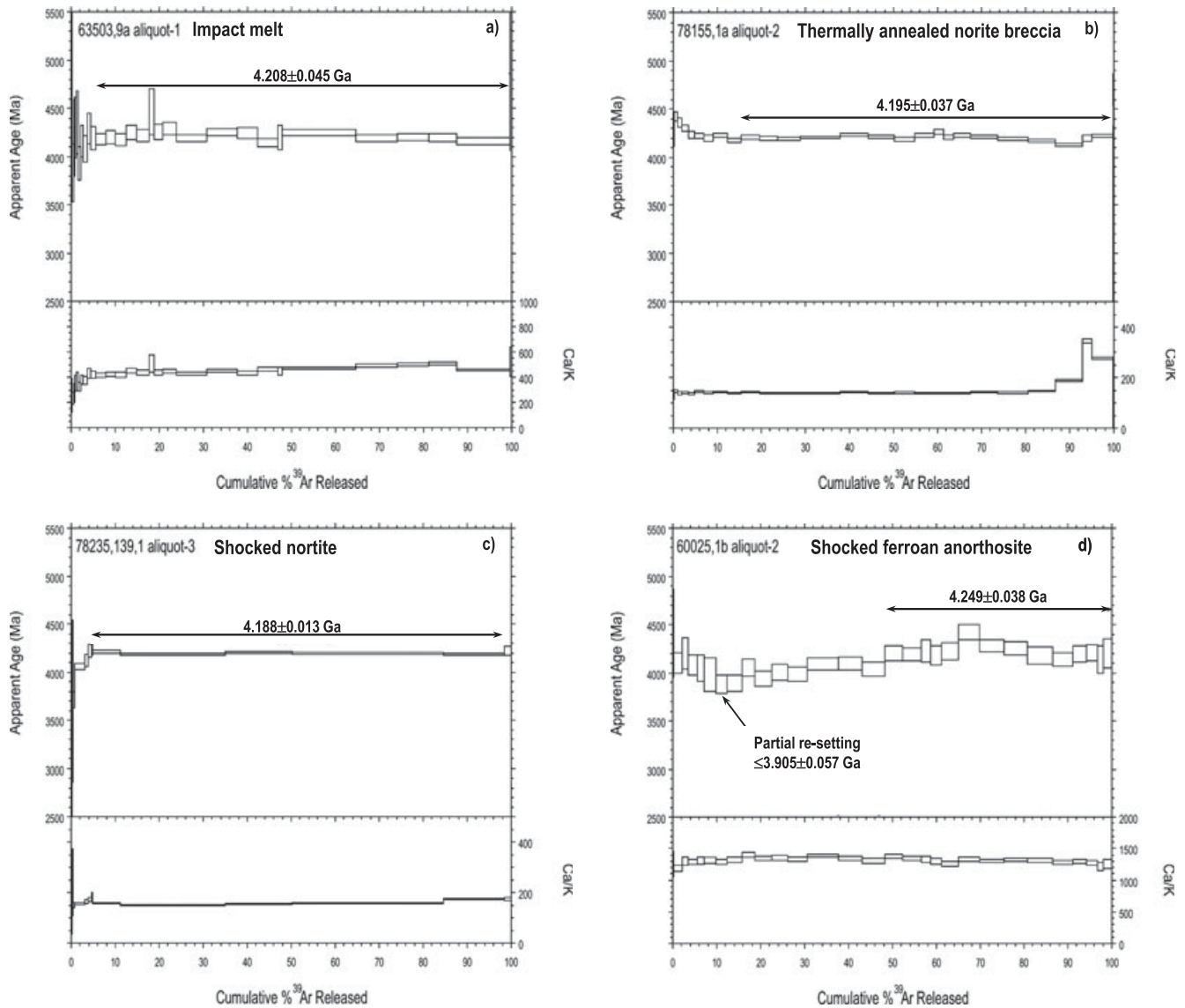
Fig. 7. $^{40}Ar/^{39}Ar$ results obtained for 13 samples from Apollo 16 and 2 samples from Apollo 17. Data presented as apparent age and Ca/K versus fraction (%) ^{39}Ar: a) 63503,9; b) 78155,1a; c) 78235,139; d) 60025; e) 63503,14; f) 63503,16; g) 63503,17; h) 63503,20; i) 63503,21; j) 63503,1; k) 63503,4; l) 63503,11; m) 63503,13; n) 63503,15; o) 63503,3.

2004; Fritz et al. 2005b). However, diffusive loss of radiogenic ^{40}Ar could be induced by shock heating and later emplacement into a warm to hot ejecta blanket (330–430 °C: Fernandes and Artemieva 2012). Sustained temperatures in excess of 500 °C can lead to the development of 120° grain boundaries in plagioclase (Kruhl [2001]; and references therein). Such thermal annealing and/or recrystallization features are observed in the anorthosite 63503,14 (Fig. 4a), the anorthosites 63503,16 and -21 (Figs. 3e and 3f), the polymict breccias 63503,3 (Fig. 5b), and especially in 63053,4 (Fig. 5c), and for the polymict noritic anorthosite breccia 78155 (Bickel 1977) (Fig. 2a).

^{40}AR-^{39}AR MEASUREMENTS

$^{40}Ar/^{39}Ar$ data for 60025, 63503 soil particles, 78155 and 78235 are shown as apparent age and Ca/K (derived from $^{37}Ar_{Ca}/^{39}Ar_{K}$) Cumulative %^{39}Ar released spectra in Fig. 7. A summary of the results is given in Table 3 (errors at 1σ level of uncertainty) and the complete data set is presented in Appendix S3 of the Online Supporting Material. This is the first report of argon data for rake samples 63503,14, -16, -17, -20, and -,21. Part of the argon data for soil fragments 63503,1, -,3, -,4, -,9, -,11, -,13, and -,15 discussed below were previously used for diffusion calculations to address post-Imbrium partial resetting of
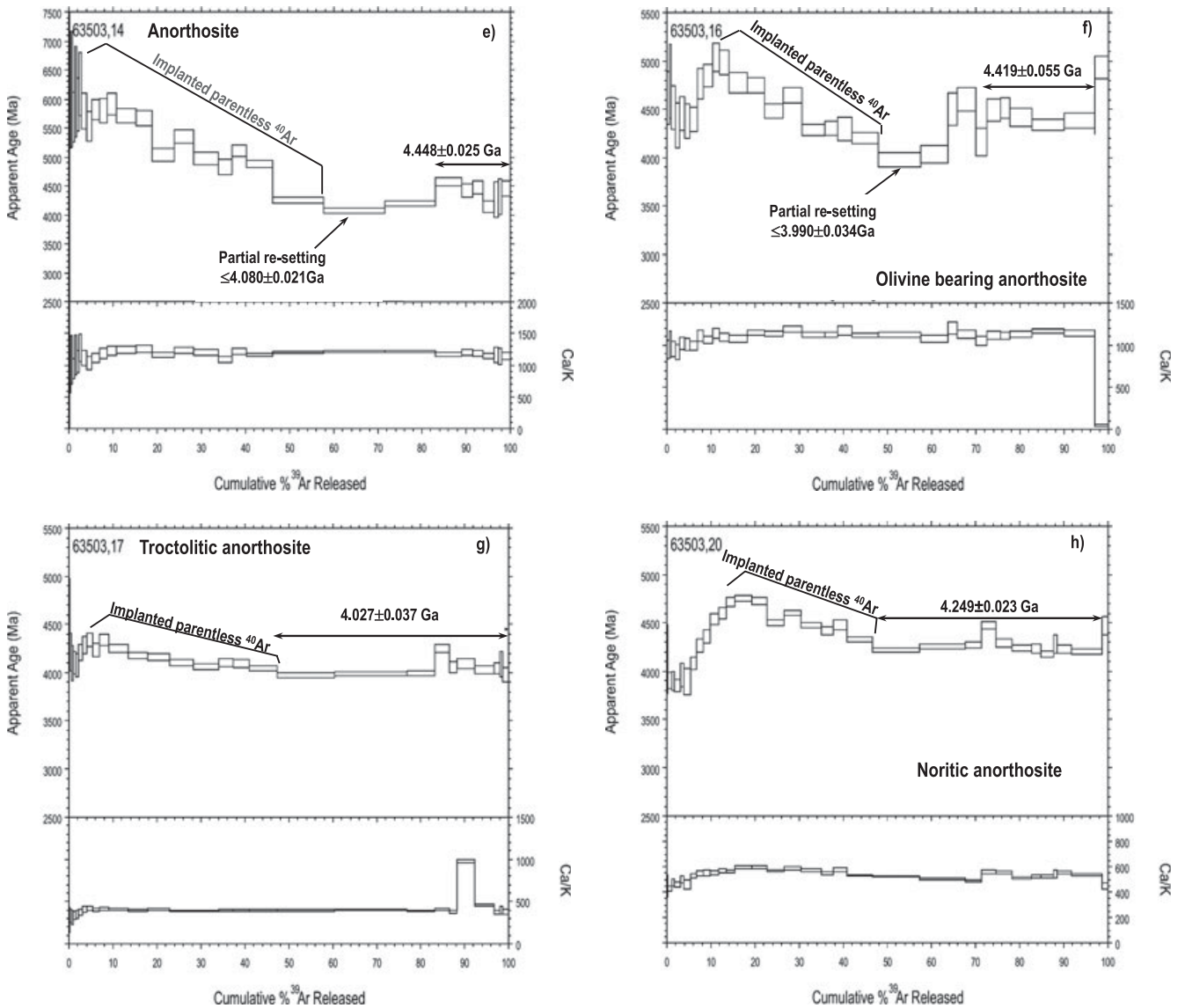
Fig. 7. *Continued.*

the K-Ar systematics (Shuster et al. 2010). Here are presented the argon release spectra together with first petrographic and geochemical data with the aim to investigate the pre- and post-Imbrium impact history. This approach is required for discriminating between crystallization and impact-reset Ar ages and for placing the ancient high-temperature release ages into a geological context. Bulk chemical composition will be used to derive the appropriate cosmic ray production rates for each sample, a requirement for calculating the best estimate for cosmic ray exposure (CRE) ages. To aid in intrepreting the high-resolution Ar step heating release patterns of thermally affected Apollo samples, the weakly shocked rock 60025, the strongly shocked rock 78235, and thermally annealed breccia 78155 were also analyzed.

The ^{40}Ar-^{39}Ar release data obtained for the 15 Apollo samples are divided into three main groups based on their release pattern for ease and condensation of data description. The reported "plateau" ages are based on consecutive intermediate and high-temperature heating steps, which are dominated by radiogenic ^{40}Ar, their apparent ages are consistent, and have no trapped component as determined from ^{36}Ar/^{40}Ar versus ^{39}Ar/^{40}Ar plots (not shown). The argon comprising these steps contained only radiogenic ^{40}Ar and some cosmogenic ^{36}Ar confirmed by the cosmogenic ^{38}Ar/^{36}Ar value for these steps. The lower ^{40}Ar/K ratios observed at low release temperatures of several samples are interpreted as indicating the maximum apparent age for the most recent argon loss event. Cosmic-ray
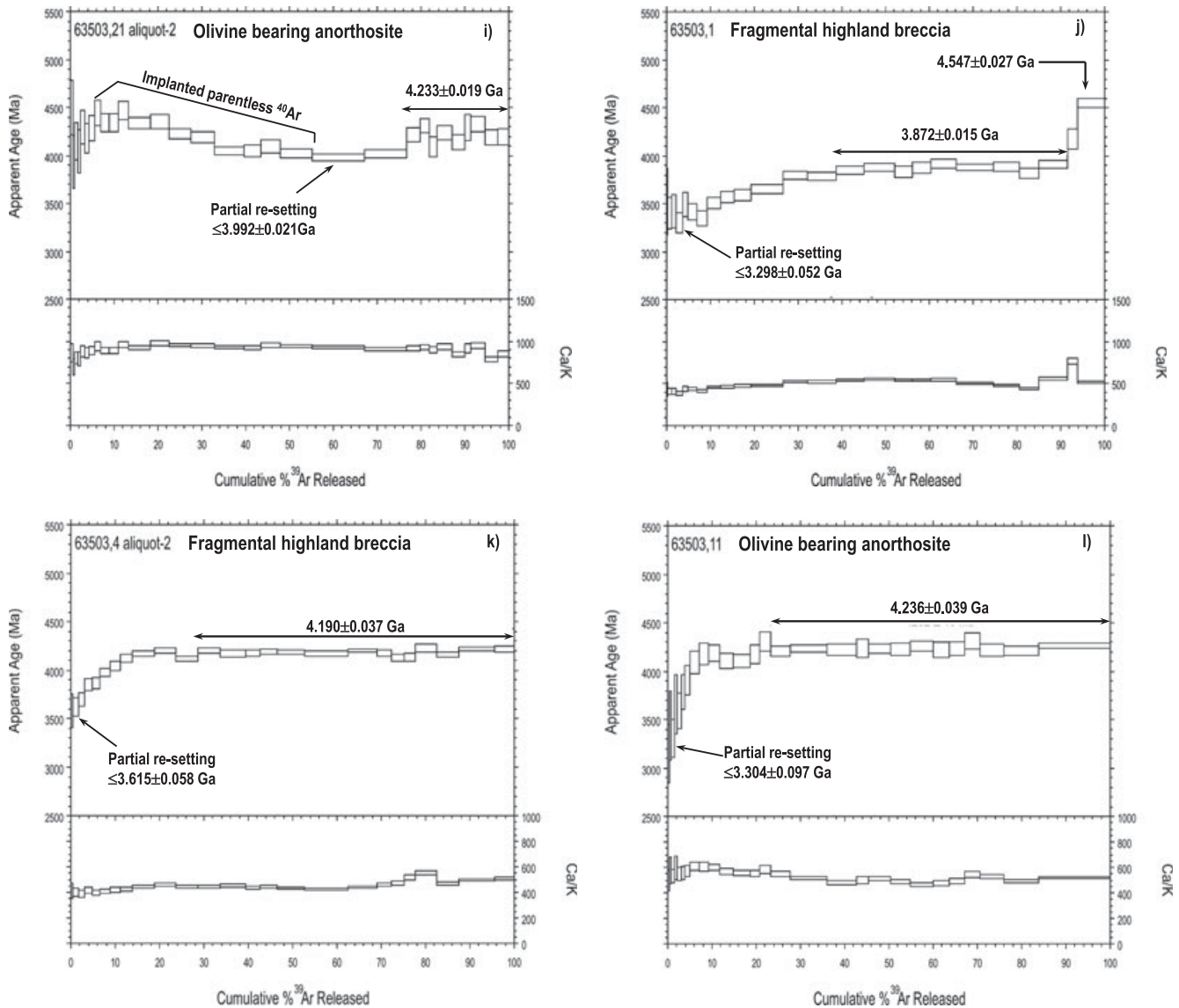
Fig. 7. *Continued.*

exposure ages, reported below and summarized in Table 3, were calculated using 2π geometry for the ^{38}Ar production rates based on bulk rock composition (Eugster and Michel 1995) determined from the mineral modal abundance (Table 1) and chemical composition (Appendix S2).

Crystallization and Impact Ages

The argon release for fragments *63503,9, 78155,1 and 78235,139* is straightforward and shows a plateau over 85–95% of the total ^{39}Ar-release (Figs. 7a–c; Table 3). The ^{40}Ar released over this release interval is solely radiogenic, and the $^{38}Ar/^{36}Ar$ over these steps shows a mixture between solar wind and cosmogenic components. The initial 5–15% ^{39}Ar-released at low temperatures suggests a small contribution from excess/parentless (or adsorbed) ^{40}Ar, and thus the ages determined for these steps have no geologic meaning. The ages calculated at intermediate and high temperatures are 4.208 ± 0.045 Ga (63503,9), 4.194 ± 0.037 Ga (averaged over four aliquots of 78155; Fig. 7b shows one of the aliquots), and 4.188 ± 0.013 Ga (78235). These ages are indistinguishable from previously reported ^{40}Ar-^{39}Ar ages (corrected for monitor age and the K-decay constant where applicable; Steiger and Jäger 1977) obtained for fragments of soil 63503 (Maurer et al. 1978), 78235 (Nyquist et al. 1981; Aeschlimann et al. 1982) and 78155 (Turner and Cadogan 1975; Oberli et al. 1979; Hudgins et al. 2008).
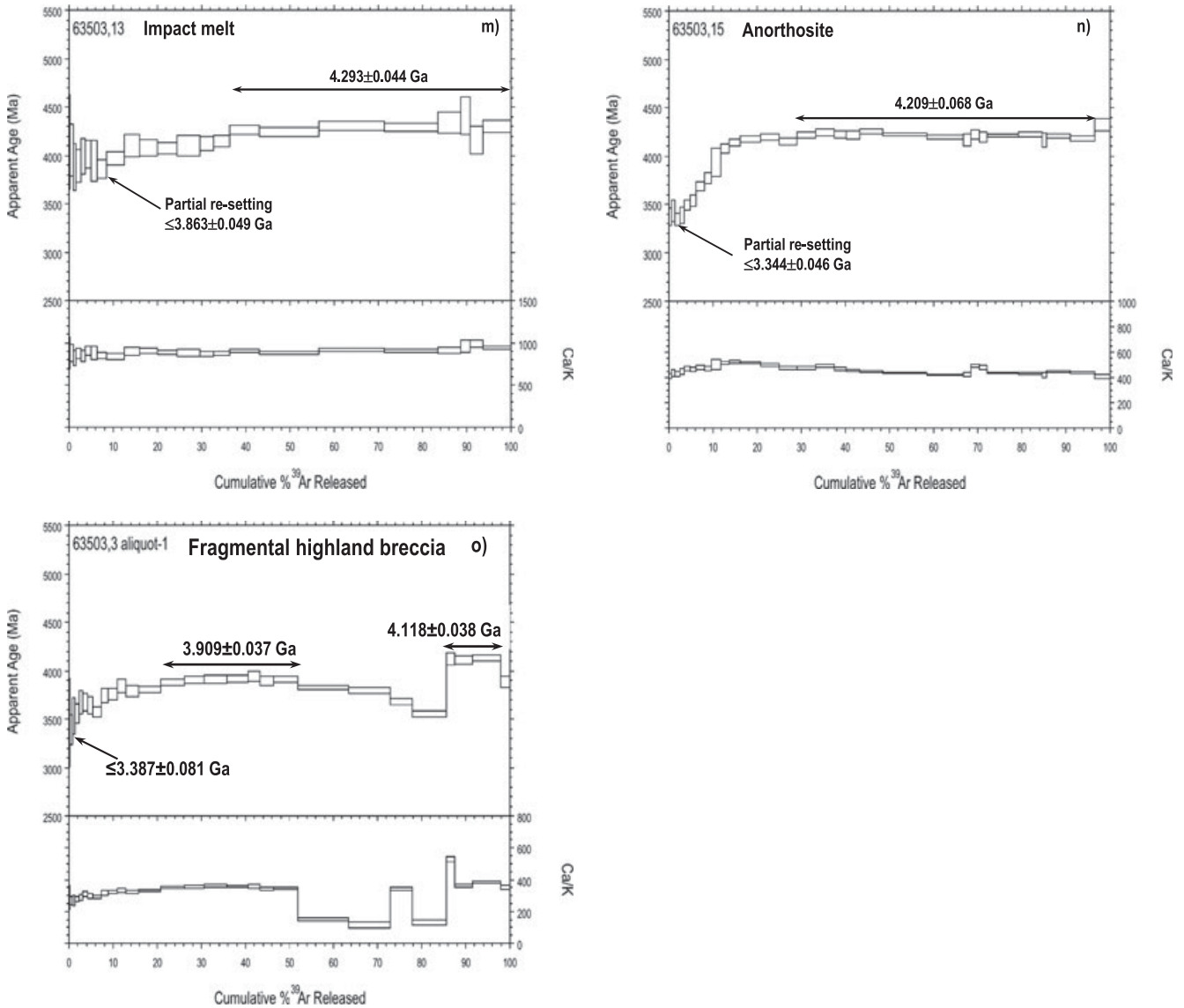
Fig. 7. *Continued.*

60025, 63503,14, 63503,16, 63503,17, 63503,20 and 63503,21 (Figs. 7d–i; Table 3). The age spectra of these samples suggest that the Ar release shows one or more shock-related phenomena, such as implantation and partial degassing of argon. The initial approximately 50% of ^{39}Ar release is dominated by trapped ^{40}Ar/^{36}Ar (0.54–1.46) and corresponds to geologically meaningless old apparent ages. These ages are initially as high as 6.0 Ga and are followed by a decrease to ages of approximately 3.91 Ga to approximately 4.3 Ga at intermediate temperatures. This is then followed by a plateau comprised only of radiogenic ^{40}Ar, with a constant Ca/K, and a total ^{39}Ar release between 23% and 53%. Two samples show evidence for only one thermal event at 4.027 ± 0.037 Ga (63503,17; Fig. 7g) and 4.249 ± 0.023 Ga (63503,20; Fig. 7h). There are

three samples suggesting two distinct events at intermediate- (*i*) and high- (*h*) temperature heating steps, 63503,14 (*i* = ≤ 4.080 ± 0.021 Ga and *h* = 4.448 ± 0.025 Ga; Fig. 7e), 63503,16 (*i* = ≤ 3.990 ± 0.034 Ga and *h* = 4.419 ± 0.055 Ga; Fig. 7f) and 63503,21 (*i* = ≤ 3.992 ± 0.021 Ga and *h* = 4.233 ± 0.019 Ga; Fig. 7i), Table 3. The high-temperature ages of 4.448 ± 0.025 Ga for 63503,14 (approximately 16% ^{39}Ar release; Fig. 7e) and of 4.419 ± 0.055 Ga for 63503,16 (approximately 24% ^{39}Ar release; Fig. 7f) suggest these to be a relic crystallization age of the primary crustal rock and the younger ages suggest the time in which these samples underwent an episode of partial degassing. The ages reported for sample 63503,21 (Fig. 7i) do not suggest an older crystallization age. Instead, the approximately 4.23 Ga age is

interpreted as a cooling event (equivocal as to whether this is a primary crystallization age or a later event) and the younger age likely a partial degassing event such as an impact. Sample 60025 shows during the first approximately 10% ^{39}Ar release a small effect of implanted argon yielding relatively high apparent ages. These ages decrease to a minimum of 3.905 ± 0.057 Ga, which is interpreted as the maximum age of a partial degassing event. For the last approximately 53% of ^{39}Ar release, an age of 4.249 ± 0.038 Ga is calculated. The effects of the implanted argon observed in the low-temperature steps can be corrected to some extent if a value for trapped ^{40}Ar/^{36}Ar is assumed within reasonable values for the lunar environment (e.g., 0–3). The trapped component is not the same for each of the affected steps of any one sample, and it decreases as the heating temperature increases (which is evident by the relatively older apparent ages from the onset of the argon release and their decrease with increase in heating temperature). It is feasible that this effect is due to fractionation of preshock radiogenic ^{40}Ar that is outgassed during impact heating and then re-implanted back into minerals. During shock implantation, the excess ^{40}Ar is injected into the rock, and its emplacement decreases into more retentive regions of the material. Thus, the effect of old apparent ages decreases with increase in temperature.

63503,1, 63503,4, 63503,11, 63503,13, 63503,15 (Figs. 7j–n). The samples in this group show that approximately 25–40% of the argon release at low temperature was partially disturbed by a thermal event (e.g., impact). There are three impact ages suggested based on this initial ^{39}Ar release, ≤ 3.3 Ga (63503,1, 63503,11, and 63503,15; Figs. 7j, 7l, and 7n), ≤3.6 Ga (63503,4; Fig. 7k), and ≤ 3.9 Ga (63503,13; Fig. 7m). At intermediate to high temperature heating steps, well-defined plateaux over approximately 60–70% of the ^{39}Ar release correspond to ages of 4.190 ± 0.037 Ga (63503, 4; Fig. 7k), 4.293 ± 0.044 Ga (63503,13; Fig. 7m), 4.236 ± 0.039 Ga (63503,11; Fig. 7l), and 4.209 ± 0.068 Ga (63503,15; Fig. 7n). Sample 63503,1 (a feldspathic fragmental breccia) shows, at intermediate and high-temperature steps (approximately 51% ^{39}Ar-release), an age of 3.872 ± 0.015 Ga (Fig. 7k). The maximum apparent age of 4.547 ± 0.027 Ga is observed for the last heating step. This last heating step might hint at a minimum crystallization age of a more retentive clast within this regolith fragment.

Finally, the release of polymict feldspathic breccia *63503,3* is complex and suggests 2–3 thermal events (Fig. 7o). Some of the effects observed in the release pattern are likely due to the nature of this sample, which is probably comprised by clasts with different composition and/or grain size as evidenced by the Ca/K

spectrum. The oldest event at 4.118 ± 0.038 Ga is recorded by the high-temperature release comprising approximately 12% of the ^{39}Ar release. The intermediate temperature steps suggest a second thermal event at 3.909 ± 0.037 Ga (approximately 26% of the total ^{39}Ar release), and the initial argon release steps suggest a partial degassing at ≤ 3.387 ± 0.081 Ga.

In summary, the ^{40}Ar-^{39}Ar data collected in this work (Table 3) for 13 fragments from Apollo 16 and 2 from Apollo 17 suggest that five crustal rocks (soil fragments 63503,11, -,15, -,21, and rocks 78155 and 78235), two lithic breccias (63503,3 and -,4) and two impact melts (63503,9 and -,13) record thermal events at ~4.2 Ga and ~4.3 Ga. Two other fragments of crustal material, 60025 and 63503,20, also have relatively older ages at ~4.25 Ga. Anorthosites 63503,16 and 63503,14 have a maximum apparent ^{40}Ar-^{39}Ar age for the last heating step at ~4.4 Ga. Similarly, breccia 63503,1 also shows a relic apparent age of ~4.55 Ga. Four crustal rocks and one impact melt (60025, 63503,13, -,14, -,17 and -,21) also suggest a later partial resetting between 3.9 and 4.0 Ga. A single breccia (63503,4) has evidence of a partial resetting at ~3.6 Ga. Two other crustal rocks and two breccias (63503,1, -,3 -,11, -,15) show an even later partial resetting at approximately 3.3 Ga, as discussed in detail by Shuster et al. (2010). Thus, these ages are likely recording several resetting events that occurred in the vicinity of Apollo 16 and Apollo 17 landing sites and/or by far away basin-forming events.

Cosmic Ray Exposure (CRE) Ages of the Apollo 16 and Apollo 17 Fragments

Determination of CRE ages of the individual fragments presents similar challenges to ^{40}Ar-^{39}Ar age determination due to the existence of cosmogenic, trapped, and nucleogenic ^{38}Ar components, the latter being formed by neutron absorption by ^{39}K during the irradiation procedure. The presence of ^{39}K-derived ^{38}Ar was corrected by the irradiation interference ratios as specified in the Methods section. Samples containing a mixture of trapped and cosmogenic ^{38}Ar have ^{38}Ar/^{36}Ar values of between 0.187 and 1.54, respectively. CRE ages are summarized in Table 3 and were calculated from the ^{38}Ar/^{37}Ar values obtained for the total release and for high-temperature steps when most of the ^{37}Ar is released. For 14 of the samples analyzed, 2π geometry (lunar surface) for ^{38}Ar production rates (P_{38}) were determined using the approach suggested by Eugster and Michel (1995), which takes into consideration the bulk rock (in this case fragment) chemical composition (bulk Ca, Fe, Ti, K, Cr, and Ni). Using this approach, the cosmogenic ^{38}Ar is not derived 100% from Ca (the main producer of ^{38}Ar); instead, the Ca contribution varied

Table 3. Summary of ^{40}Ar-^{39}Ar age results for Apollo 16 and Apollo 17 samples analyzed in this study. Errors are 1σ level of uncertainty.

Lithology		Sample wt (mg)	K[a] (ppm)	Max. age at high-T (Ga) [^{39}Ar%]	Early event (Ga) [^{39}Ar%]	Later event (Ga)	2π CRE-age (Ma)
Apollo 16							
Crustal Rock							
60025,1,b	Anorthosite	0.42	224	4.44 ± 0.02[b] 4.36 ± 0.02[c]	4.249 ± 0.038 [53]	≤3.905 ± 0.057	2.1 ± 0.3
63503,14	Anorthosite	0.55	74	4.448 ± 0.025 [16]	4.080 ± 0.021	–	55 ± 3
63503,16	Anorthosite	0.65	51	4.419 ± 0.055 [24]	–	≤3.990 ± 0.034	60 ± 5
63503,17	Anorthositic troctolite	0.65	636	–	4.027 ± 0.037 [39]	–	261 ± 5
63503,20	Anorthosite	0.82	142	–	4.249 ± 0.023 [52]	–	126 ± 8
63503,21	Anorthosite	–	67	–	4.233 ± 0.019 [20]	≤3.992 ± 0.021	46 ± 1
63503,11	Anorthosite	0.53	197	–	4.236 ± 0.039 [75]	≤3.304 ± 0.097	51 ± 1
63503,15	Anorthosite	0.50	330	–	4.209 ± 0.068 [63]	≤3.344 ± 0.046	46 ± 2
Breccia							
63503,1	Polymict breccia	0.86	235	4.547 ± 0.027[d]	3.872 ± 0.015 [51]	≤3.298 ± 0.052	53 ± 2
63503,3	Polymict breccia	0.81	226	4.118 ± 0.038 [12]	3.909 ± 0.037	≤3.387 ± 0.081	46 ± 2
63503,4	Polymict breccia	1.18	191	–	4.190 ± 0.037 [71]	≤3.615 ± 0.058	45 ± 2
Impact melt							
63503,9,a	Anorthosite	0.50	748	–	4.208 ± 0.045	–	43 ± 3
63503,13	Noritic anorthosite	0.53	101	–	4.293 ± 0.044 [59]	≤3.863 ± 0.049	346 ± 10
Apollo 17							
Crustal Rock							
78155 (×4)	Noritic anorthosite	0.39–0.85	730	–	4.195 ± 0.037 [88]	–	17 ± 1
78235,139,1	Norite	0.64	610	4.43 ± 0.05[e]	4.188 ± 0.013 [94]	–	262 ± 5

[a]Bulk K content reported was calculated based on the average chemical composition of plagioclase, pyroxene, and olivine obtained by EMP (Appendix S2) and the modal abundance of these minerals (Table 1).
[b]Sm/Nd age determined by Carlson and Lugmair (1988).
[c]Sm/Nd and Pb/Pb age determined by Borg et al. (2011).
[d]Maximum apparent age comprised of the last step at high-temperature and likely the minimum crystallization age of the primary rock.
[e]Sm/Nd age determined by Nyquist et al. (1981).

between 68% and 97%. The remainder ^{38}Ar production came from the minor contributors (Fe, Ti, K, Cr, and Ni), which caused an overall lowering of the production rate. The bulk composition for samples 60025, 78155, and 7825 were taken from the literature (Nakamura et al. 1973; Rose et al. 1973; Winzer et al. 1975; Higuchi and Morgan 1975; Wänke et al. 1976, 1977). The bulk composition for fragments from soil 63503 was estimated based on the mineral modal abundance and respective mineral chemical composition as listed in Table 1 and Appendix S2. The P_{38} varied from 0.9 to 1.0×10^{-8} cm^3 g^{-1} Ca Ma^{-1}. The exception was the fragmental breccia 63503,1, for which there are no pyroxene and olivine chemical composition data. Because the mineral modal abundance for breccia 63503,1 is similar to that of 63503,20, the same $P_{38} = 0.914 \times 10^{-8}$ cm^3 g^{-1} Ca Ma^{-1} was used to calculate the CRE-age of 63503,1. It is worth noting that
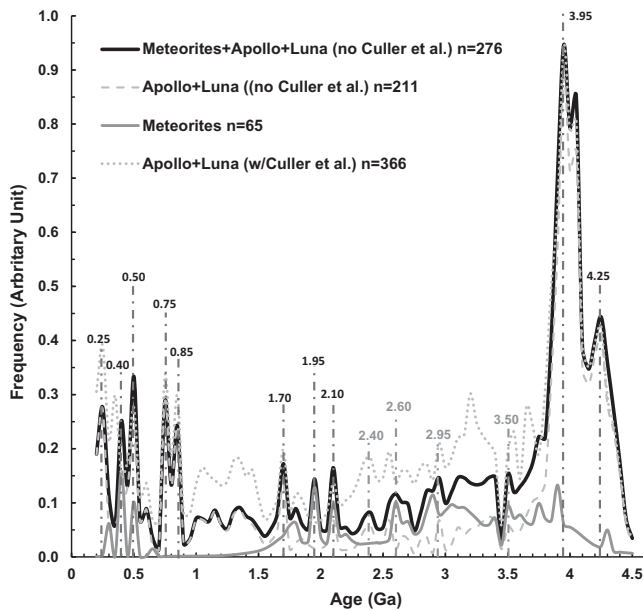
Fig. 8. Gaussian probability curve calculated using published $^{40}Ar/^{39}Ar$ impact ages obtained for samples from Apollo 12, 14, 16, and 17 and Luna 16 and 24 missions (this work; Kirsten et al. 1973; Schaeffer and Husain 1973, 1974; Kirsten and Horn 1974; Cadogan and Turner 1976, 1977; Schaeffer and Schaeffer 1977; Maurer et al. 1978; McGee et al. 1978; Staudacher et al. 1978; Dalrymple and Ryder 1996; Culler et al. 2000; Levine et al. 2005; Barra et al. 2006; Norman et al. 2006, 2007; Zellner et al. 2006; Hudgins et al. 2008) and lunar meteorites (Fernandes et al. 2000, 2004, 2008, 2009; Daubar et al. 2002; Gnos et al. 2004; Cohen et al. 2005; Takeda et al. 2006; Burgess et al. 2007; Haloda et al. 2009; Sokol et al. 2008; Joy et al. 2011). To calculate this curve, the age and error were combined in bins of 0.05 Ga (50 Ma), which is representative of the average error in $^{40}Ar/^{39}Ar$ age determination. The normalized Gaussian curve calculated for each age bin (age column) was obtained by taking into consideration the width of the Gaussian curve calculated and the measured uncertainties. Each column was added and the result normalized to an integer. This integer was used to normalize all curves shown in the diagram. Thus, the height of the curve/peak (y-axis) reflects the relative frequency of a certain age (x-axis). Where necessary, the age was corrected for monitor age and decay-constant. The thick black line is the cumulative impact ages for Apollo, Luna, and meteorites and does not include the Culler et al. (2000) data (see main text). However, for comparison, the same curve with the Culler et al. (2000) data is plotted and shown using the thin dotted line. The black vertical lines indicate the time of flux increases that are better deconvolved with the current available data. The gray vertical lines are only suggestive of potential increase in the impact flux.

shielding depth is not accounted for; thus, currently, it is not possible to directly evaluate whether all the fragments have experienced different burial histories.

For the present sample set of 12 fragments from soil 63503, 9 of these fragments representing different lithologies show a prevalent age of approximately 50 Ma. This is in agreement with previously determined CRE-ages for Apollo 16 fragments from 63503 soil reported by Arvidson et al. (1975) and Maurer et al. (1978) and assigned to the event that excavated the North Ray crater. Other studies suggest younger CRE ages (Schaeffer and Husain 1973; Shuster et al. 2010). The younger CRE ages reported for the same fragments by Shuster et al. (2010) resulted from a calculation using a ^{38}Ar production rate based on the assumption that the cosmogenic ^{38}Ar was all produced from Ca (it was not included the input from other elements) and the P_{38} was calculated for a 4π geometry scenario. This led to an overestimation of the P_{38} and therefore the younger ages reported in the Shuster et al. (2010). The CRE ages reported here (Table 3) suggest that most of the fragments in soil 63503 have remained in the same vicinity since they were exposed by the event that excavated the North Ray crater at approximately 50 Ma and were not exposed to cosmic rays prior to their excavation wherever they resided. Three other fragments from soil 63503 (samples 63503,13, -,17 and -,20) have CRE ages between 126 and 346 Ma, suggesting a longer exposure to cosmic radiation, and thus a different history as regolith components. The cosmic ray exposure age of approximately 2 Ma calculated for the ferroan anorthosite 60025 is in agreement with previous reports and suggested as ejecta from the South Ray crater (Arvidson et al. 1975; Drozd et al. 1977).

CRE ages for the two Apollo 17 rocks analyzed suggest an age of 17 Ma for 78155, which is similar to that reported by Hudgins et al. (2008), but younger than that reported by Turner and Cadogan (1975). Finally, the CRE age determined for 78235 is calculated to be 262 Ma and similar to that previously reported by Drozd et al. (1977) using the ^{81}Kr-Kr method.

DISCUSSION

The K/Ar ages of the measured Apollo samples range between 4.547 ± 0.027 and $\leq 3.298 \pm 0.052$ Ga. They are, thus, opening a window to the impact flux onto the Earth–Moon system prior to the putative lunar cataclysm centered around approximately 3.9 Ga. Therefore, the petrologic and chronologic data obtained from the Apollo 16 and Apollo 17 samples will be discussed in the context of lunar impact history.

The Ancient Lunar Crust

An older apparent age of 4.547 ± 0.027 Ga observed in this study was obtained from the highest temperature step of the feldspathic fragmental breccia 63503,1 (Fig. 7j). Preservation of such an ancient age would be in agreement with the lack of thermal

annealing features in this breccia (i.e., the temperature was low enough to allow some fragments in the breccia to preserve an old, relic age). Previously, Jessberger et al. (1974) reported ages on sample 65015, a poikilitic melt with relic lithic fragments showing at the high-temperature steps a similar argon-release pattern and old age to that obtained for soil fragment 63503,1. The broad plateau in the intermediate temperature step during 63503,1 Ar release provides an age of 3.872 ± 0.015 Ga that probably marks the formation of the breccia. Later at $\leq 3.298 \pm 0.052$ Ga, the breccia experienced a minor thermal event (see also Shuster et al. 2010), which caused the observed partial resetting at low temperature (Fig. 7j). Thus, this fragment bears witness to the first approximately 1.3 Ga of the Earth–Moon system.

Four of the ten crustal fragments investigated (Table 3) suggest the preservation of old crystallization ages: Sm/Nd and Pb/Pb age for rock 60025 (4.44–4.36 Ga) are reported by Carlson and Lugmair (1988) and Borg et al. (2011). For 78235, an age of 4.43 Ga is reported (Nyquist et al. 1981), Table 3, and recent Sm-Nd investigations on the paired samples 78236 and 78238 (Nyquist et al. 2008; Edmunson et al. 2009; respectively) have suggested a somewhat younger crystallization age of approximately 4.33 Ga. Similarly, relic ages of 4.45 and 4.42 Ga are preserved at the high-temperature steps during Ar release for two Apollo 16 soil samples 63503,14, and 63503,16, respectively. These four samples also show the effects of later (younger) thermal events (Table 3) at 4.3, 4.2, 4.0, and 3.9 Ga, which will be discussed in the following sections.

Impact Ages of 4.3–4.2 Ga Observed in Different Lithologies and Landing Sites

Ar ages in the range of 4.3–4.2 Ga were determined from a total of 11 of 15 Apollo 16 and Apollo 17 samples analyzed. Therefore, these ages provide insights into the likely irregular increases in the impact flux during the overall decline of the available material for these events, and possibly not just one large peak at approximately 3.9 Ga (see also Husain and Schaeffer 1975). Impact-related Ar ages of 4.2 and 4.3 Ga are clearly obtained from impact melt fragments 63503,9 and -,13, respectively; the completely recrystallized fragmental breccia 63503,4; and the thermally annealed breccia 78155. The fragmental breccia 63503,3, although not completely recrystallized, contains abundant impact melt fragments and recrystallized regions in its matrix. This suggests that the 4.118 ± 0.038 Ga Ar age for high-temperature steps in this breccia dates an impact event on the Moon and a later brecciation event at 3.909 ± 0.037 Ga. The breccia was later partially

degassed by a thermal event at ≤ 3.4 Ga. Thus, these impact-reset rocks demonstrate that impact ages of 4.2 and 4.3 Ga are still preserved on different localities of the lunar surface.

Evidence for impact-resetting is less clear for the remaining samples. Anorthositic troctolite 63503,17 has an Ar age of 4.027 ± 0.037 Ga, and the FAN fragments 63503,11, -,15, -,20, and -,21, have maximum $^{40}Ar/^{39}Ar$ ages around 4.25 Ga comprising 23–76% of the ^{39}Ar release at intermediate and high step-heating temperatures. The approximately 4.2 Ga Ar ages obtained for the FANs 63503,11, -,15, -,20, and -,21 are consistent with corrected (Hb3gr monitor age—Turner 1971; Renne et al. 1998; Schwarz and Trieloff 2007— and K-decay constant: Steiger and Jäger 1977) $^{40}Ar/^{39}Ar$ ages obtained by Maurer et al. (1978), Schaeffer and Husain (1973), and Norman et al. (2006, 2007) on fragments found in the soil from Apollo 16 in the vicinity of the North Ray crater (Stations 11 and 13). However, none of the latter 63503 show well-developed annealing features (see the Petrography and Chemistry of the Apollo 16 and Apollo 17 Samples section). Meanwhile, FAN rock 60025 (collected close to the lunar module) has an ancient Sm-Nd and Pb/Pb age (4.44 Ga: Carlson and Lugmair 1988; 4.36 Ga Borg et al. 2011), but a younger $^{40}Ar/^{39}Ar$ age (Fig. 7d; Table 3). Similarly, the 4.43 Sm-Nd age of Apollo 17 rock 78235 (Nyquist et al. 1981) is older than the $^{40}Ar/^{39}Ar$ ages from the intermediate and high-temperature Ar-release steps (Fig. 7c; Table 3). Thus, the $^{40}Ar/^{39}Ar$ ages for Apollo 17 rock 78235 and Apollo 16 rock 60025 are not dating the crystallization of these rocks at 4.2 and 4.25 Ga, respectively, but instead a later complete resetting of the K-Ar system due to a thermal disturbance. Nonetheless, neither shock nor annealing features (see the Petrological Constraints on the Thermal History section and Table 2) are sufficiently developed in these samples to be consistent with resetting of the Ar ages. In addition, the lack of well-developed annealing features (e.g., granoblastic to granulitic texture) in norite 78235 and anorthosites 60025, 63503,11, -,15 and -,20 does not provide petrological evidence for a complete resetting of the Ar ages (e.g., instead, the probable emplacement of cold rock fragments into a hot ejecta blanket). An extended exposure to moderate temperatures (i.e., 330–430 °C) cannot be excluded (Fernandes and Artemieva 2012).

Formation Age and/or Impact Exhumation Age

To explain the relatively young Ar ages of weakly thermally annealed FAN rocks and the discrepancy in ages measured by other isotopic chronometers, an impact exhumation scenario is discussed that considers 1)

crystallization in deep and warm crustal levels with open-system behavior for some isotopic systems, and 2) exhumation of this deep-seated crustal material by basin-forming impacts and cooling on or near the lunar surface.

The age discrepancy between Sm-Nd and K-Ar data measured in the norite 78235 (see Table 3) was proposed by Nyquist et al. (1981) to be caused by a two-stage cooling history: initial crystallization at approximately 4.4 Ga deep within the lunar crust where temperatures (e.g., Spohn et al. 2001; Meyer et al. 2010) remained above the closure temperature of the K-Ar system and a later cooling to lunar surface temperatures at the time the rock was exhumed by a basin-forming event (~4.2 Ga). Identical conclusions were derived earlier by Wilshire (1974) and Jackson et al. (1975) who suggested that this rock was formed at depths of 8–30 km and exhumed by a large basin-forming event.

Sm-Nd analyses by Carlson and Lugmair (1981) on samples 73244,27,45 (a noritic clast within a polymict breccia) and 67667 (a feldspathic lherzolite) gave similar ages at approximately 4.2 Ga. These authors suggested that either the 4.2 Ga age was due to prolonged endogenous igneous activity that produced plutonic rocks for an extended period of the lunar early history or due to the age of an event that exhumed material from deep within the lunar crust (see also Snyder et al. 2000; Nemchin et al. 2008). In this latter case, the rock was maintained "warm" and likely in an area where temperatures exceeded the Sm/Nd closure temperature (>1000 °C: Carlson and Lugmair 1981b).

Similarly, several attempts to acquire a crystallization age for troctolite 76535 using different radiogenic systems (Sm/Nd, Rb/Sr, U/Pb, and K/Ar: Husain and Schaeffer 1975; Huneke and Wasserburg 1975; Bogard et al. 1975; Papanastassiou and Wasserburg 1976; Lugmair et al. 1976; Premo and Tatsumoto 1992; Hinthorne et al. 1975) suggest a crystallization age of approximately 4.2 Ga. More recently, Nyquist et al. (2012), in a work where the age of this rock was revisited, argued for an older Sm/Nd age of 4.34 ± 0.071 Ga. McCallum et al. (2006) conducted cooling rates experiments on orthopyroxenes from troctolite 76535. These experiments suggested that this troctolite was exhumed from the lower crust where it was maintained at temperatures above the closure temperatures for Sm-Nd, U-Pb, and Ar-Ar isotopic systems. These temperatures were kept by heat diffusing from concentrations of U- and Th-rich KREEP material at the base of the crust.

This impact exhumation scenario can also explain the difference between the Sm-Nd crystallization age and the K-Ar age for some FAN rocks (e.g., 60025 with crystallization at 4.44 Ga and resetting of the K-Ar system at approximately 4.2 Ga; Carlson and Lugmair 1988; Schaeffer and Husain 1973, 1974; and this work).

It could also explain the 4.36 Ga Pb-Pb age, and 4.32 Ga ^{146}Sm-^{142}Nd ages reported recently for 60025 (Borg et al. 2011) within the petrological context of the standard lunar magma ocean (LMO) model. The standard LMO model (Shearer et al. [2006] and references therein) interprets FAN rocks as flotation cumulates that formed during crystallization of the LMO. Following the assumption that FAN rock 60025 is an LMO product, it formed earlier than the 4.36 Ga Pb-Pb ages. The LMO crystallization is constrained to have been completed before 4.42 Ga ago, as given by the isotopic age of the KREEP reservoir (Shearer et al. 2006; Nemchin et al. 2009a). The impact excavation model could explain the isotopic age of FAN rocks being younger than the reservoir age of the KREEP source. FAN rock 60025 could have formed early (>4.42 Ga) during the LMO crystallization at deep crustal levels where temperatures remained for an extended period of time above the closing temperatures of the different isotopic systems.

Impact-induced emplacement of material from more than 20 km depth is expected. For example, Wieczorek and Phillips (1999) calculated that the Nectaris impact exhumed material from up to 45 km depth onto the lunar surface. Stöffler et al. (1985) calculated that 30% of the Nectaris ejecta reaching the Apollo 16 site came from >20 km crustal depth. Thus, impact exhumation of hot crustal material onto the lunar surface should be considered especially for basin-forming events during the early lunar history, a period characterized by a higher thermal gradient within the lunar crust compared with today (Spohn et al. 2001; Meyer et al. 2010).

In the context of the 4.2–4.3 Ga Ar ages recorded in Apollo 16 and Apollo 17 samples, it is interesting to note that U-Pb analyses of zircons found in Apollo 14 and Apollo 17 breccias by Pidgeon et al. (2007), Nemchin et al. (2008, 2009b), and Grange et al. (2009) were interpreted as peaks in the lunar impact flux at approximately 4.2 and 4.3 Ga, which probably induced periods of enhanced KREEP magmatism. It is also likely that prior to the earlier peak reported here (~4.3 Ga), there were other peaks that affected this region of the solar system.

Younger Resetting Ages at 4.0, 3.9, 3.6, and 3.3 Ga

The ^{40}Ar/^{39}Ar measurements of the 63503 soil fragments reported here also permitted the identification of ages probably representing other partial resetting thermal events. Four of the fragments suggest a partial resetting at approximately 4.0 Ga, three at approximately ~3.9 Ga, one at 3.6 Ga, and four at 3.3 Ga (this latter event is further explored by Shuster et al. 2010). Together with the 4.3 and 4.2 Ga peaks,

these more recent peaks suggest that the impact flux onto the Earth–Moon system is complex.

This complexity of the impact flux can be explored by compiling the literature data into an age Gaussian probability curve. Figure 8 shows a compilation of a total of 276 ^{40}Ar/^{39}Ar impact ages from Apollo and Luna samples (this work; Kirsten et al. 1973; Schaeffer and Husain 1973, 1974; Kirsten and Horn 1974; Cadogan and Turner 1976, 1977; Schaeffer and Schaeffer 1977; Maurer et al. 1978; McGee et al. 1978; Staudacher et al. 1978; Dalrymple and Ryder 1996; Culler et al. 2000; Levine et al. 2005; Barra et al. 2006; Norman et al. 2006, 2007; Zellner et al. 2006; Hudgins et al. 2008) as well as lunar meteorites (Fernandes et al. 2000, 2004, 2008, 2009; Daubar et al. 2002; Gnos et al. 2004; Cohen et al. 2005; Takeda et al. 2006; Burgess et al. 2007; Haloda et al. 2009; Sokol et al. 2008; Joy et al. 2011). To calculate the Gaussian probability curve, and ease in plotting the curve, the age bins were used with widths of 0.05 Ga (50 Ma), which is a conservative average of the error in ^{40}Ar/^{39}Ar age determination. The normalized Gaussian curve calculated for each age bin (age column) was obtained by taking into consideration the width of the Gaussian curve calculated and the measured uncertainties. Each column was added and the result normalized to an integer. This integer was used to normalize all curves shown in Fig. 8. Thus, the height of the curve/peak (*y*-axis) reflects the relative frequency of a certain age (*x*-axis). Where necessary, the literature ages were corrected for monitor age and K-decay constant (Steiger and Jäger 1977). The thick black line in Fig. 8 is the cumulative impact ages of samples from for Apollo and Luna missions and lunar meteorites. This black line does not include the Culler et al. (2000) data as there is no chemical composition information for the glasses dated by these authors (such that it is not possible to distinguish whether the glasses dated are either of impact or volcanic origin). This line suggests that the data from a total of 65 impact-related ages extracted from different lunar meteorites and 211 impact-related ages acquired from the Apollo and Luna samples represent a complex impact flux from 4.5 to 0.2 Ga. The largest peak is noticeable at approximately 3.92 Ga as observed in the lunar literature; however other peaks at 4.3, 4.2, 4.0, 3.9, [3.5, 3.3, 2.9, 2.4], 2.1, 1.95, 1.7, [1.35, 1.05], 0.85, 0.75, 0.50, 0.40 and 0.25 Ga are also resolvable in the cumulative curve. This Gaussian curve is by no means the final representation of the Moon impact history; however, it corresponds to the current data set and what can be deconvolved from what is presently available. As more impact-reset ages become available and earlier literature ages are corrected for K-decay

constant and monitor samples age, it will be possible to derive peaks with better age accuracy. Nonetheless, a Gaussian probability curve diagram provides an overview of the available data, and factors influencing data availability and representativeness are to be considered while interpreting these spikes.

Thus, the reason for the dominant peak at approximately 3.9 Ga can either be due to the large number of impacts onto the lunar surface around this time (i.e., Turner et al. 1973; Tera et al. 1974), or alternatively due to a higher availability of material with this age at the Apollo (and Luna) landing sites (Baldwin 1974; Haskin 1998). This bias could be due to the fact that the samples were collected over a restricted and surficial area of the Moon.

Sample Bias and the Continuous Gardening of the Lunar Surface

With the advent of remote sensing data obtained from satellites orbiting the Moon (e.g., Clementine and Lunar Prospector, Chandrayaan-1 missions), it has been possible to make global chemical maps of lunar surface chemistry (Lawrence et al. 1998; Elphic et al. 2000; Gillis et al. 2003, 2004; Prettyman et al. 2006). With these global chemical maps, it is obvious that the terrains surrounding most of the Apollo landing sites have a similar composition (Haskin 1998; Korotev 2000) and probably are not representative of the whole Moon. Most of the surface in the region where the Apollo landing sites were located is affected by the KREEP signature of the ejecta excavated by the event that created the Imbrium Basin. In addition to KREEP, the Mg-suite rocks (including norites, troctolites, dunites, and alkali anorthosites) are also considered to concentrate within the Procellarum-KREEP Terrane (PKT) (Korotev 2005).

Different authors (e.g., Haskin 1998; Korotev 2000; Baldwin 1974, 2006) suggest that most of the Apollo mission landing sites contain material that was ejected by the impact that formed the Imbrium Basin (e.g., Fra Mauro and Cayley formations) and distributed material over a large region of the lunar nearside and possibly some to the lunar farside (Petro and Pieters 2006; Hood and Artemieva 2008). The three Luna missions landed farther east of the PKT and so are potentially less contaminated by Imbrium Basin ejecta material.

Another parameter is the decline in impact flux after approximately 3.9 Ga. Considering the large amount of ejecta produced during the formation of basins around this time (or possibly ending at this time) followed by a comparatively lower impact flux, it is expected that the predominance of material on the lunar surface with the ~3.9 Ga age signature overwhelms the ages obtained

from material at any one locality. Moreover, the lower impact flux and decrease in impactor size implies comparatively less mixing of the upper regolith and likely comparatively minor mixing with deeper megaregolith. Thus, the more recent (and smaller) events dominate gardening and the ejecta material at the top of the stratigraphic column of any lunar area. As a result, the top of the lunar stratigraphic column will contain less older/earlier impact-reset materials (see fig. 3 in Hartmann 2003). In contrast, the record of older events is likely to be preserved in deeper stratigraphic layers of the lunar regolith, probably at depths greater than the deepest core drilled during the Apollo 17 mission (~3 m). Petro and Pieters (2006) modeled the range of megaregolith thickness to be between 800 and 1000 m in the region surrounding the Imbrium Basin, which is capped by regolith with a thickness of approximately 100 m (Hartmann 2003) and composed of comminuted rocks. It is probable that some of the samples collected by the Apollo and Luna missions came from deeper stratigraphic layers, such as those collected on impact ejecta of small craters and reflecting material from older basins. This is the case of samples collected from the ejecta of North Ray crater, which is approximately 230 m deep and is the source of the samples analyzed in this study.

Considering the estimated depths of formation of regolith and megaregolith and the possible decrease in the impact rate of the lunar surface through time, it is currently difficult to have a good estimate of the temporal lunar impact flux; essentially because the samples were obtained from the lunar surface or from relatively shallow depths such as those acquired by the Apollo (and Luna) missions. Hence, the mixing of rocks with different reset ages will be focused more on regolith affected by more recent events. This will cause the decrease in abundance of rocks showing reset ages during the initial 600 Ma. Nevertheless, the present work demonstrates that rock material from the ejecta blanket of the young (50 Ma) North Ray crater record pre-3.9 Ga impacts preserved in stratigraphically deeper layers of the lunar regolith. Samples that have been ejected from other relatively young impact craters may also preserve an archive of >3.9 Ga impact events and should be sampled by future missions to the Moon to provide a more complete understanding of the ancient impact bombardment. Finally, the lunar meteorites represent samples from upper layers of the lunar regolith (possibly deeper than the Apollo and Luna samples). In contrast with Apollo mission samples, which were restricted to the lunar equatorial nearside, the lunar meteorites probably originated from various random locations from several meters depth, and, thus, are considered to be more representative of the lateral composition and history of the lunar surface. The age distribution of impact melt clasts in meteorites does not show a dominance of the 3.9 Ga age, but it shows several peaks in the range between approximately 4.3 and 2.5 Ga (Fig. 8) (Chapman et al. 2007). The impact age distribution shown by the lunar meteorites does not support a "terminal lunar cataclysm." Instead, it appears to show that the age distribution for the samples obtained by Apollo and Luna missions is biased toward a predominance of ~3.9 Ga ages.

The Descartes Formation

To place the diverse lithologies with 4.2 Ga ages obtained in this study into a selenological context, we briefly revisit the previous work on the Descartes Formation and its relation to the Nectaris Basin. The ejecta from the North Ray crater (Stations 11 and 13) is considered to have excavated material of the Descartes Formation (Stöffler et al. 1985). Whether the Descartes Formation was emplaced or reworked by either Nectaris or Imbrium ejecta is still controversial (see James 1981; Stöffler et al. [2006] and references therein; Norman et al. 2010). However, samples from the Apollo 16 landing site, and especially those collected at Stations 11 and 13, have been used to date the Nectaris Basin. Presently, the age range proposed for Nectaris is between 4.2 Ga (Schaeffer et al. 1976) and 3.85 Ga (Schaeffer et al. 1985).

Based on Sm/Nd and Rb/Sr (Nyquist and Wiesmann 1981; Reimold et al. 1985) and Ar/Ar ages (Schaeffer et al. 1976) of several rocks inferred to be from the Descartes Formation, an age of 4.1–4.2 Ga for Nectaris was proposed by Schaeffer et al. (1976), Reimold and Nieber-Reimold (1984) and Reimold et al. (1985).

Maurer et al. (1978) reported Ar ages of KREEP-free fragments clustering around 4.2 Ga (now decay-constant-corrected [Steiger and Jäger 1977]), and KREEP-rich fragments clustering around 3.9 Ga. On the basis of the working hypothesis that the KREEP layer was globally distributed under the lunar crust and excavated by multiple basin-sized impact events, Maurer et al. (1978) concluded that the 4.2 Ga cluster represents a series of impacts smaller than basin-sized impacts. The 3.9 Ga cluster was suggested by Maurer et al. (1978) to represent a series of basin-sized impacts including Nectaris and Imbrium. This line of reasoning is called into question by the Lunar Prospector mission that provided global elemental maps revealing that KREEP material is almost exclusively restricted to the PKT region (Lawrence et al. 1998; Prettyman et al. 2006) and by implication was distributed to all Apollo landing sites mainly by the Imbrium (Haskin et al. 1998; Norman et al. 2010) and possibly Serenitatis

impacts, but not by the Nectaris event. Except for one plagioclase fragment in impact melt rock 63503,9 with high K values (approximately 1100 ppm), all the studied samples display low bulk K contents (50–750 ppm; Table 3) showing that no KREEP signature was identified in the studied rocks. However, a KREEP-like signature in a rock with a 4.2 Ga Sm-Nd isochron was also reported for breccia 67955 collected at the rim of the North Ray crater (Norman et al. 2007).

A popular line of argument for the age of Nectaris Basin relies on the formation ages of fragmental breccia rocks collected on the rim of the North Ray crater. James (1981) argued that a 3.9 Ga age for the Descartes Formation, and by implication the Nectaris impact, is provided by the formation ages of these breccias (i.e., being equal to or younger than the youngest clast within these breccias). Later, a consortium study of Apollo 16 samples revealed ages for these fragmental breccias as young as 3.85 Ga (Stöffler et al. [1985] and references therein). However, a 3.85 Ga age for Nectaris would be in conflict with identical ages proposed for the stratigraphically younger Imbrium Basin (see Stöffler et al. 2006). Deutsch and Stöffler (1987) tried to resolve these inconsistencies by dating the Imbrium impact to an age of 3.77 Ga. Norman et al. (2010) conducted geochemical and Ar-Ar chronological work on the fragmental breccias 67016 and 67455 collected from the rim of the North Ray crater. These authors identified KREEP-rich impact melt rock clasts with ages of 3.85 Ga interpreted to be their time of formation by the Imbrium event. They concluded that fragmental breccias collected at the rim of the North Ray crater provide no chronological information for assigning an age to the Nectaris impact. This could imply that either the Descartes Formation is part of the Imbrium ejecta (Norman et al. 2010), or the formation of these breccias is not related to the emplacement of the Descartes Formation.

Relating individual samples collected from the lunar surface with a specific impact basin will always be ambiguous to some extent. However, the basins Tranquilitatis, Nectaris, and Serentitatis substantially contributed to the substratum forming the Apollo 16 landing site (Petro and Pieters 2006) and, thus, probably are represented by impact-reset ages for rocks in the Apollo 16 sample collection. This work confirms the $^{40}Ar/^{39}Ar$ studies of Schaeffer et al. (1976) and Maurer et al. (1978) by showing that 4.2–4.3 Ga old impact-reset rock fragments were collected by Apollo 16 astronauts. This shows that impact-reset rocks as old as 4.2–4.3 Ga substantially contribute to the Descartes Formation, which covers a wide area of the lunar surface.

Assigning an age of 4.2 Ga to a large basin like Nectaris (Schaeffer et al. 1976; Reimold and Nieber-

Reimold 1984; Reimold et al. 1985; Warren 2003) and/or Tranquilitatis and Serentitatis would be implicit from impact excavation models (see the Formation Age and/or Impact Exhumation Age section) and consistent with the viscosity arguments presented by Baldwin (1974, 2006). Baldwin (1974, 2006) argued that the ages of lunar basins can be deduced by comparing the topographic relief of the impact structures (categorized from young to old corresponding to class 1–10, respectively). Older crater structures (>161 km diameter) that formed in a less viscous (warmer) lunar crust would display a higher degree of topographic smoothing compared with younger crater structures that formed on a cooler and thus a more supportive lunar crust. Baldwin (1974, 2006) argued that the prominent morphological differences in Orientale (class 2) and Nectaris (class 7) require the later basin to be older by a few 100 Ma.

A less viscous (warmer) crust impacted by the Tranquilitatis, Nectaris, or Serentitatis projectile would corroborate the interpretation that the 4.2 Ga Ar ages of FAN rocks date the time at which the material was excavated from warm deep crustal levels and subsequently cooled below the Ar-closure temperature on the lunar surface (see the Formation Age and/or Impact Exhumation Age section).

Ancient Impact Ages and Implications for the Age of South Pole Aitken Basin

The available impact record dates back to approximately 4.3 Ga ago (this work; Schaeffer and Husain 1973, 1974; Schaeffer et al. 1976; Maurer et al. 1978; Nyquist et al. 1981; Carlson and Lugmair 1981; Nemchin et al. 2008, 2009; Pidgeon et al. 2007; Grange et al. 2009). Independent from assigning a specific source crater or basin to the different impact rocks, the ages of the oldest impact melt rocks may constrain the formation age of the oldest impact structures. The SPA Basin presents not only the oldest but also the largest impact basin on the Moon identified by photo-geological investigations of the lunar surface (Wilhelms 1987). Although there may be basins older than the SPA (Frey 2011), we consider it less probable that several impact-reset rocks from pre-SPA impact craters were collected by different Apollo missions. If so, the ages of the oldest impact melt rocks provide constraints for the youngest possible age for the SPA impact event. Hence, we hypothesize that the South Pole-Aitken Basin is equal to or older than 4.293 ± 0.044 Ga as given by the high-temperature steps of the intersertal impact melt rock 63503,13 (Table 3). An ancient age for SPA (≥4.3 Ga) is supported by the fact that this giant basin

(approximately 2500 km) is more than twice the size of the second largest basin, Imbrium (approximately 1150 km). The apparent gap in basin size may indicate that the SPA formed by a different population of projectiles compared with those forming the majority of younger and substantially smaller basins. A very early formation age of SPA and some of the stratigraphically younger lunar basins would be consistent with very large impact events before 4.0 Ga ago on other parent bodies, as documented by (1) impact ages >4.4 Ga in HED meteorites (Bogard and Garrison 2003), (2) H-chondrites (Fernandes et al. 2006; Swindle et al. [2009] and references therein), (3) IAB iron-meteorites (Vogel and Renne 2008), (4) GRA 06129 (Shearer et al. 2010; Fernandes and Shearer 2010), (5) impact ages >4.35 Ga in enstatite chondrites (Bogard et al. 2010), (6) impact ages of 4.27 Ga in LL-chondrites (Trieloff et al. 1989, 1994; Dixon et al. 2004), (7) 4.20 Ga in Bencubbin meteorite (Marty et al. 2010), (8) 4.1 Ga in ureilitic meteorites (Bogard and Garrison 1994), and (9) a 4.1 Ga age for the Martian ALH 84001 (Ash et al. 1996; Turner et al. 1997; Bogard and Garrison 1999; Cassata et al. 2010). As a great variety of impact events older than 4.0 Ga ago are recorded in a variety of parent bodies, it is expected that the Moon did not escape impacts during this early period.

CONCLUSIONS

The 15 samples studied comprise three major lithologic types: crustal rocks, breccias, and impact melt rocks. Within the crustal material, the range of rock types was FAN, olivine-bearing anorthosite, noritic anorthosite, and an anorthositic troctolite. The $^{40}Ar/^{39}Ar$ data obtained for 15 Apollo fragments (13 from Apollo 16 and 2 from Apollo 17) witness an extended period of lunar geologic history. These fragments probably preserve not only a relic crystallization age but also partial and total resetting of the K-Ar clock due to later thermal events.

The polymict feldspathic fragmental breccias 63503,1, 63503,3, and 63503,4 display different degrees of thermal overprinting: breccia 63503,1 hints at the preservation of a relict Ar age of 4.547 ± 0.027 Ga, and the strongly recrystallized 63503,4 was completely reset at approximately 4.2 Ga. Two impact melt rocks developed different igneous textures caused by differences in their cooling times. The quickly quenched impact melt 63503,9 represents molten ejecta from an impact crater that formed approximately 4.2 Ga ago. In contrast, the crystallized impact melt rock 63503,13 probably cooled inside a melt pond (~4.3 Ga), with a later impact at approximately 3.9 Ga delivering the rock fragment to the Apollo 16 landing site.

The observed shock features and the deduced shock temperatures are not sufficient to explain substantial to complete resetting of the K-Ar chronometer. An extended period at elevated temperatures (i.e., in a hot ejecta blanket) could cause the resetting of the K-Ar clock (e.g., Fernandes and Artemieva 2012). Alternatively, the apparent Ar ages (and their younger ages relative to their Sm-Nd ages) could be explained by exhumation of hot crustal material from deep crustal levels (e.g., 20–45 km) onto the lunar surface and subsequent cooling below the Ar-closing temperature. Interpreting the 4.3–4.2 Ga ages of Apollo 16 anorthosites as impact exhumation ages directly implies that these ages relate to a large and likely basin-forming impact event(s) (e.g., Tranquillitatis, Serenitatis, and Nectaris). Interestingly, two Apollo 17 samples analyzed in this work also recorded a thermal event (i.e., impact) at approximately 4.2 Ga, further suggesting that either this event was large enough so that its ejecta were spread over a radius of at least approximately 1000 km or that there were more than one impacts on the Moon at this time.

A compilation of 280 $^{40}Ar/^{39}Ar$ of lunar samples (literature data and this work; see Fig. 8) indicates a complex impact history of the Earth–Moon system with events at 4.3, 4.2, 4.0, 3.9, [3.5, 3.3, 2.9, 2.4], 2.1, 1.95, 1.7, [1.35, 1.05], 0.85, 0.75, 0.50, 0.40, and 0.25 Ga. To better understand this early period of the inner solar system, further work will be necessary on samples collected by the Apollo and Luna missions as well as samples from other regions of the Moon. Thus, future missions should be planned for locations afar from the PKT regions and collected with improved geologic contextual information.

The deepest drilling depth cored during the Apollo missions was just approximately 3 m (Apollo 17: 70001–70006). The samples collected at Apollo 16 Stations 11 and 13, which were naturally excavated from an estimated depth of approximately 230 m, are therefore likely samples from the deepest stratigraphic level of the lunar regolith sampled by the Apollo (and Luna) missions. Several of the fragments from this site give K-Ar ages older than the approximately 3.9 Ga (a period thought to have had a high impact flux), and thus the ejecta blanket of the North Ray crater serves as a window to an older period of the Earth–Moon early history (and inner solar system). This highlights an important caveat when dealing with Apollo samples: the likely stratigraphic and compositional bias imposed by the samples. Samples collected during the Apollo missions were mostly from the lunar surface, and thus probably showing the effects of the more recent large thermal event (e.g., at 3.9 Ga).

Based on the oldest $^{40}Ar/^{39}Ar$ age obtained for an impact melt (4.293 ± 0.044 Ga) and those reported for

zircons by Nemchin et al. (2008, 2009), Pidgeon et al. (2007), and Grange et al. (2009) and interpreted as due to resetting events, the present work suggests a possible minimum age of the SPA Basin. The age of this basin is argued to be ≥ 4.3 Ga because the oldest impact melt rock recovered from the lunar surface provides the minimum age for the oldest lunar impact structure. It appears that the Earth–Moon system during its initial 600 Myr was probably affected by different periods of increased impact bombardment (i.e., peaks) during the overall decrease in the impact size and rate over time.

Editorial Handling—Dr. Ian Lyon

REFERENCES

Aeschlimann U., Eberhardt P., Geiss J., Grogler N., Kurtz J., and Marti K. 1982. On the age of cumulate norite 78236 (abstract). 13th Lunar and Planetary Science Conference. p. 1.

Artemieva N. A. and Ivanov B. 2004. Launch of Martian meteorites in oblique impacts. *Icarus* 171:84–101.

Arvidson R., Crozaz G., Drozd R. J., Hohenberg C. M., and Morgan C. J. 1975. Cosmic ray exposure ages of features and events at the Apollo landing sites. *The Moon* 13:259–276.

Ash R. D., Knott S. F., and Turner G. 1996. A 4-Gyr shock age for a Martian meteorite and implications for the cratering history of Mars. *Nature* 380:57–59.

Baldwin R. B. 1974. Was there a 'terminal lunar cataclysm' 3.9 to 4.0 billion years ago. *Icarus* 23:157–166.

Baldwin R. B. 2006. Was there ever a terminal lunar cataclysm? With lunar viscosity arguments. *Icarus* 184:308–318.

Barra F., Swindle T. D., Korotev R. L., Jolliff B. L., Zeigler R. A., and Olson E. 2006. ^{40}Ar-^{39}Ar dating of Apollo 12 regolith: Implications for the age of Copernicus and the source of nonmare materials. *Geochimica et Cosmochimica Acta* 70:6016–6031.

Bickel C. E. 1977. Petrology of 78155: An early, thermally metamorphosed polymict breccia. Proceedings, 8th Lunar Science Conference, p. 2007.

Bogard D. 1995. Impact ages of meteorites: A synthesis. *Meteoritics* 30:244–268.

Bogard D. D. and Garrison D. H. 1994. ^{39}Ar-^{40}Ar ages of four ureilites (abstract). 24th Lunar and Planetary Science Conference. pp. 137–138.

Bogard D. D. and Garrison D. H. 1999. Argon-39-argon-40 "ages" and trapped argon in Martian Shergottites, Chassigny, and Allan Hills 84001. *Meteoritics & Planetary Science* 34:451–473.

Bogard D. D. and Garrison D. H. 2003. ^{39}Ar-^{40}Ar ages of eucrites and thermal history of asteroid 4 Vesta. *Meteoritics & Planetary Science* 38:669–710.

Bogard D. D., Nyquist L. E., Shih C. Y., Bansal B. M., and Wiesmann H. 1975. 76535—an old lunar rock. *Earth and Planetary Science Letters* 26:69–80.

Bogard D. D., Dixon E. T., and Garrison D. H. 2010. Ar-Ar ages and thermal histories of enstatite meteorites. *Meteoritics & Planetary Science* 45:723–742.

Borg L. E., Connelly J. N., Boyet M., and Carlson R. W. 2011. Chronological evidence that the Moon is either young or did not have a global magma ocean. *Nature* 477:70–72.

Bottke W. F., Levison H. F., Nesvorný D., and Dones L. 2007. Can planetesimals left over from terrestrial planet formation produce the lunar late heavy bombardment? *Icarus* 190:203–223.

Bouvier A. and Wadhwa M. 2010. The age of the solar system redefined by the oldest Pb–Pb age of a meteoritic inclusion. *Nature Geoscience* 3:637–641.

Brereton N. R. 1972. A reappraisal of the ^{40}Ar/^{39}Ar stepwise degassing technique. *Geophysical Journal of the Royal Astronomical Society* 27:449–478.

Burgess R. and Turner G. 1998. Laser ^{40}Ar-^{39}Ar age determinations of Luna 24 mare basalts. *Meteoritics & Planetary Science* 33:921–935.

Burgess R., Fernandes V. A., Irving A. J., and Bunch T.E. 2007. Ar-Ar ages of NWA 2977 and NWA 3160—Lunar meteorites paired with NWA 773 (abstract #1603). 38th Lunar and Planetary Science Conference. CD-ROM.

Cadogan P. H. and Turner G. 1976. The chronology of the Apollo 17 Station 6 boulder. Proceedings, 7th Lunar Science Conference. pp. 2267–2285.

Cadogan P. H. and Turner G. 1977. ^{40}Ar-^{39}Ar dating of Luna 16 and Luna 20 samples. *Philosophical Transactions of the Royal Society of London* 284:167–177.

Carlson R. W. and Lugmair G. W. 1981a. Time and duration of lunar highlands crust formation. *Earth and Planetary Science Letters* 52:227–238.

Carlson R. W. and Lugmair G. W. 1981b. Sm-Nd age of lherzolite 67667: Implications for the processes involved in lunar crustal formation. *Earth and Planetary Science Letters* 56:1–8.

Carlson R. W. and Lugmair G. W. 1988. The age of ferroan anorthosite 60025: Oldest crust on a young Moon? *Earth and Planetary Science Letters* 90:119–130.

Cassata W. S., Renne P. R., and Shuster D. L. 2009. Argon diffusion in plagioclase and implications for thermochronometry: A case study from the Bushveld Complex, South Africa. *Geochimica et Cosmochimica Acta* 73:6600–6612.

Cassata W. S., Shuster D. L., Renne P. R., and Weiss B. P. 2010. Evidence for shock heating and constraints on Martian surface temperatures revealed by ^{40}Ar/^{39}Ar thermochronometry of Martian meteorites. *Geochimica et Cosmochimica Acta* 74:6900–6920.

Chapman C. R., Cohen B. A., and Grinspoon D. H. 2007. What are the real constraints on the existence and magnitude of the late heavy bombardment? *Icarus* 189:233–245.

Cohen B. A., Swindle T. D., and Kring D. A. 2005. Geochemistry and ^{40}Ar-^{39}Ar geochronology of impact-melt clasts in feldspathic lunar meteorites: Implications for lunar bombardment history. *Meteoritics & Planetary Science* 40:755–777.

Culler T. S., Becker T. A., Muller R. A., and Renne P. R. 2000. Lunar impact history from ^{40}Ar/^{39}Ar dating of glass spherules. *Science* 287:1785–1788.

Dalrymple G. B. and Ryder G. 1996. Argon-40/argon-39 age spectra of Apollo 17 highlands breccia samples by laser step heating and the age of the Serenitatis Basin. *Journal of Geophysical Research* 101:26069–26084.

Dalrymple G. B., Alexander E. C., Lanphere M. A., and Kraker G. P. 1981. Irradiation of samples for ^{40}Ar/^{39}Ar dating using Geological Survey TRIGA reactor. U.S. Geological Survey Professional Paper 1176. Reston, Virginia: U.S. Geological Survey.

Daubar I. J., Kring D. A., Swindle T. D., and Jull A. J. T. 2002. Northwest Africa 482: A crystalline impact-melt breccia from the lunar highlands. *Meteoritics & Planetary Science* 37:1797–1813.

Deutsch A. and Stöffler D. 1987. Rb-Sr-analyses of Apollo 16 melt rocks and a new age estimate for the Imbrium Basin: Lunar basin chronology and the early heavy bombardment of the moon. *Geochimica et Cosmochimica Acta* 51:1951–1964.

Dixon J. and Papike J. J. 1975. Petrology of anorthosites from the Descartes region of the Moon: Apollo 16. Proceedings, 6th Lunar Science Conference. pp. 263–291.

Dixon E. T., Bogard D. D., Garrison D. H., and Rubin A. E. 2004. ^{39}Ar-^{40}Ar evidence for early impact events on the LL parent body. *Geochimica et Cosmochimica Acta* 68:3779–3790.

Drozd R. J., Hohenberg C. M., Morgan C. J., Podosek F. A., and Wroge M. L. 1977. Cosmic-ray exposure history at Taurus-Littrow. Proceedings, 8th Lunar Science Conference. pp. 3027–3043.

Edmunson J., Borg L. E., Nyquist L. E., and Asmerom Y. 2009. A combined Sm–Nd, Rb–Sr, and U-Pb isotopic study of Mg-suite norite 78238: Further evidence for early differentiation of the Moon. *Geochimica et Cosmochimica Acta* 73:514–527.

Elphic R. C., Lawrence D. J., Feldman W. C., Barraclough B. L., Maurice S., Binder A. B., and Lucey P. G. 2000. Lunar rare earth element distribution and ramifications for FeO and TiO$_2$: Lunar Prospector neutron spectrometer observations. *Journal of Geophysical Research* 105:20333–20346.

Eugster O. and Michel T. 1995. Common asteroid breakup events of eucrites, diogenites, and howardites, and cosmic-ray production rates for noble gases in chondrites. *Geochimica et Cosmochimica Acta* 59:177–199.

Fernandes V. A. and Artemieva N. 2012. Impact ejecta temperature profile on the Moon—What are the effects on the Ar-Ar dating method? (abstract #1367). 43rd Lunar and Planetary Science Conference. CD-ROM.

Fernandes V. A. and Burgess R. 2005. Volcanism in Mare Fecunditatis and Mare Crisium: Ar-Ar age studies. *Geochimica et Cosmochimica Acta* 69:4919–4934.

Fernandes V. A. S. M. and Shearer C. K. 2010. ^{40}Ar-^{39}Ar ages of metamorphism preserved in the achondrite GRA 06129 (abstract #1008). 41st Lunar and Planetary Science Conference. CD-ROM.

Fernandes V. A., Burgess R., and Turner G. 2000. Laser ^{40}Ar/^{39}Ar age studies of Dar al Gani 262 Lunar meteorite. *Meteoritics & Planetary Science* 35:1355–1364.

Fernandes V. A., Burgess R., and Turner G. 2003. Ar-Ar chronology of lunar meteorites Northwest Africa 032 and 773. *Meteoritics & Planetary Science* 38:555–564.

Fernandes V. A., Anand M., Burgess R., and Taylor L. A. 2004. Ar-Ar studies of Dhofar clast-rich feldspathic highland meteorites: 025, 026, 280, 303 (abstract #1514). 35th Lunar and Planetary Science Conference. CD-ROM.

Fernandes V. A., Burgess R., Bischoff A., and Metzler K. 2006. Ar composition of the melt lithology within the NWA 2457 breccia (abstract #5308). 69th Meteoritical Science Conference. p. 5308.

Fernandes V., Becker T., Renne P., and Burgess R. 2008. Preliminary Ar-Ar studies of lunar basaltic meteorite Dhofar 287-A (abstract #A264). Goldschmidt Conference, Vancouver, Canada.

Fernandes V. A., Burgess R., and Morris A. 2009a. Ar-Ar age determinations of lunar basalt meteorites: Asuka 881757, Yamato 793169, Miller Range 05035, La Paz 02205, North West Africa 479, and Elephant Moraine 96008. *Meteoritics & Planetary Science* 44:805–821.

Fernandes V. A., Korotev R. L., and Renne P. R. 2009b. ^{40}Ar-^{39}Ar ages and chemical composition for lunar mare basalts: NWA 4734 and NWA 4898 (abstract #1045). 40th Lunar and Planetary Science Conference. CD-ROM.

Fernandes V. A. S. M., Fritz J. P., Wünnemann K., and Hornemann U. 2010. K-Ar ages and shock effects in lunar meteorites (abstract #EPSC2010-237). European and Planetary Science Congress. 237 p.

Frey H. V. 2011. Previously unknown large impact basins on the Moon: Implications for lunar stratigraphy. In *Recent advances and current research issues in lunar stratigraphy*, edited by Ambrose W. A. and Williams D. A. Geological Society of America Special Paper 477. Boulder, Colorado: Geological Society of America. pp. 53–75.

Fritz J., Greshake A., and Stöffler D. 2005a. Micro-Raman spectroscopy of plagioclase and maskelynite in Martian meteorites: Evidence of progressive shock metamorphism. *Antarctic Meteorite Research* 18:96–116.

Fritz J., Greshake A., and Artemieva N. 2005b. Ejection of Martian meteorites. *Meteoritics & Planetary Science* 40:1393–1411.

Gillis J. J., Jolliff B. L., and Elphic R. C. 2003. A revised algorithm for calculating TiO_2 from Clementine UVVIS data: A synthesis of rock, soil, and remotely sensed TiO_2. *Journal of Geophysical Research* 108. doi: 10.1029/2001JE001515.

Gillis J. J., Jolliff B. L., and Korotev R. L. 2004. Lunar surface geochemistry: Global concentrations of Th, K, and FeO as derived from lunar prospector and Clementine data. *Geochimica et Cosmochimica Acta* 68:3791–3805.

Gnos E., Hofmann B. A., Al-Kathiri A., Lorenzetti S., Eugster O., Whitehouse M. J., Villa I. M., Jull A. J. T., Eikenberg J., Spettel B., Krähenbühl U., Franchi I. A., and Greenwood R. C. 2004. Pinpointing the source of a lunar meteorite: Implications for the evolution of the Moon. *Science* 305:657–660.

Gomes R., Levison H. F., Tsiganis K., and Morbidelli A. 2005. Origin of the cataclysmic late heavy bombardment period of the terrestrial planets. *Nature* 435:466–469.

Grange M. L., Nemchin A. A., Pidgeon R. T., Timms N., Muhling J. R., and Kennedy A. K. 2009. Thermal history recorded by the Apollo 17 impact melt breccia 73217. *Geochimica et Cosmochimica Acta* 73:3093–3107.

Haloda J., Tycova P., Korotev R. L., Fernandes V. A., Burgess R., Jakes P., Gabzdyl P., and Kosler J. 2009. Petrology, geochemistry, and age of low-Ti mare-basalt meteorite Northeast Africa 003-A: A possible member of the Apollo 15 mare basaltic suite. *Geochimica et Cosmochimica Acta* 73:3450–3470.

Hanan B. B. and Tilton G. R. 1987. 60025—RELICT of primitive lunar crust? *Earth and Planetary Science Letters* 84:15–21.

Hartmann W. K. 1975. Lunar "cataclysm"—A misconception. *Icarus* 24:181–187.

Hartmann W. K. 2003. Megaregolith evolution and cratering cataclysm models—Lunar cataclysm as a misconception (28 years later). *Meteoritics & Planetary Science* 38:579–593.

Hartmann W. K. and Neukum G. 2001. Cratering chronology and the evolution of Mars. *Space Science Reviews* 96:165–194.

Haskin L. A. 1998. The Imbrium impact event and the thorium distribution at the lunar highlands surface. *Journal of Geophysical Research* 103:1679–1689.

Haskin L. A., Korotev R. L., Rockow K. M., and Jolliff B. L. 1998. The case for an Imbrium origin of the Apollo Th-rich impact-melt breccias. *Meteoritics & Planetary Science* 33:959–975.

Head J. W. 1974. Morphology and structure of the Taurus-Littrow highlands (Apollo 17): Evidence for their origin and evolution. *The Moon* 9:355–395.

Head J. W. 1979. Serenitatis multi-ringed basin—Regional geology and basin ring interpretation. *Moon and the Planets* 21:439–462.

Higuchi H. and Morgan J. W. 1975. Ancient meteoritic component in Apollo 17 boulders. Proceedings, 6th Lunar Science Conference. pp. 1625–1651.

Hinthorne J. R., Conrad R. L., and Andersen C. A. 1975. Lead-lead and trace element abundances in lunar troctolite, 76535. Proceedings, 6th Lunar Science Conference. pp. 373–375.

Hodges F. N. and Kushiro I. 1973. Petrology of Apollo 16 lunar highland rocks. Proceedings, 4th Lunar Science Conference. pp. 1033–1048.

Hodges C. A., Muehlberger W. R., and Ulrich G. E. 1973. Geologic setting of Apollo 16. Proceedings, 5th Lunar Science Conference. pp. 1–25.

Hood L. L. and Artemieva N. A. 2008. Antipodal effects of lunar basin-forming impacts: Initial 3D simulations and comparisons with observations. *Icarus* 193:485–502.

Hörz F., Schultz P. H., Grieve R. A. F., and Wilhelms D. E. 1981. What was the mode of emplacement of the Cayley and Descartes formations? Discussion summary. In *Workshop on Apollo 16*, edited by James O. B. and Hörz F. LPI Technical Report 81-01. Houston, Texas: Lunar and Planetary Institute. pp. 15–18.

Hudgins J. A., Spray J. G., Kelley S. P., Korotev R. L., and Sherlock S. C. 2008. A laser probe $^{40}Ar/^{39}Ar$ and INAA investigation of four Apollo granulitic breccias. *Geochimica et Cosmochimica Acta* 72:5781–5798.

Huneke J. C. and Wasserburg G. J. 1975. Trapped ^{40}Ar in troctolite 76535 and evidence for enhanced ^{40}Ar-^{39}Ar age plateaus. Proceedings, 6th Lunar Science Conference. pp. 417–419.

Husain L. and Schaeffer O. A. 1975. Lunar evolution: The first 600 million years. *Geophysical Research Letters* 2:29–32.

Jackson E. D., Sutton R. L., and Wilshire H. G. 1975. Structure and petrology of a cumulus norite boulder sampled by Apollo 17 in Taurus-Littrow Valley, the Moon. *Geological Society of America Bulletin* 86:433–442.

James O. B. 1981. ^{40}Ar-^{39}Ar ages of Apollo 16 coarse-fines fragments and the age of Nectaris (abstract). 12th Lunar and Planetary Science Conference. p. 503.

James O. B., Lindstrom M. M., and McGee J. J. 1991. Lunar ferroan anorthosite 60025: Petrology and chemistry of mafic lithologies. Proceedings, 21st Lunar and Planetary Science Conference. pp. 63–87.

Jessberger E. K., Huneke J. C., and Wasserburg G. J. 1974. Evidence for a ~ 4.5 aeon age of plagioclase clasts in a lunar highland breccia. *Nature* 248:199–202.

Jourdan F. and Renne P. 2007. Age calibration of the Fish Canyon sanidine $^{40}Ar/^{39}Ar$ dating standard using primary K-Ar standards. *Geochimica et Cosmochimica Acta* 71:387–402.

Joy K. H., Burgess R., Hinton R., Fernandes V. A., Crawford I. A., Kearsley A. T., and Irving A. J. 2011. Petrogenesis and chronology of lunar meteorite Northwest Africa 4472: A KREEPy regolith breccia from the Moon. *Geochimica et Cosmochimica Acta* 75:2420–2452.

Kirsten T. and Horn P. 1974. Chronology of the Taurus-Littrow region. III—Ages of mare basalts and highland breccias and some remarks about the interpretation of lunar highland rock ages. Proceedings, 5th Lunar Science Conference. pp. 1451–1475.

Kirsten T., Horn P., and Kiko J. 1973. ^{39}Ar-^{40}Ar dating and rare gas analysis of Apollo 16 rocks and soils. Proceedings, 4th Lunar Science Conference. pp. 1757–1784.

Korotev R. L. 1994. Compositional variation in Apollo 16 impact-melt breccias and inferences for the geology and bombardment history of the Central Highlands of the Moon. *Geochimica et Cosmochimica Acta* 58:3931–3969.

Korotev R. L. 1997. Some things we can infer about the Moon from the composition of the Apollo 16 regolith. *Meteoritics & Planetary Science* 32:447–478.

Korotev R. L. 2000. The "Great Lunar Hot Spot" and the composition and origin and origin of the Apollo mafic ("LKFM") impact-melt breccias. *Journal of Geophysical Research* 105:4317–4345.

Korotev R. L. 2005. Lunar geochemistry as told by lunar meteorites. *Chemie der Erde* 65:297–346.

Kruhl J. 2001. Crystallographic control on the development of foam textures in quartz, plagioclase and analogue material. *International Journal of Earth Sciences* 90:104–107.

Lawrence D. J., Feldman W. C., Barraclough B. L., Binder A. B., Elphic R. C., Maurice S., and Thomsen D. R. 1998. Global elemental maps of the Moon: The Lunar Prospector Gamma-Ray Spectrometer. *Science* 281:1484–1489.

Levine J., Becker T. A., Muller R. A., and Renne P. R. 2005. ^{40}Ar/^{39}Ar dating of Apollo 12 impact spherules. *Geophysical Research Letters* 32. doi:10.1029/2005GL022874.

Lugmair G. W., Marti K., Kurtz J. P., and Scheinin N. B. 1976. History and genesis of lunar troctolite 76535 or: How old is old? Proceedings, 7th Lunar Science Conference. pp. 2009–2033.

Maher K. A. and Stevenson D. J. 1988. Impact frustration of the origin of life. *Nature* 331:612–614.

Marty B., Kelley S., and Turner G. 2010. Chronology and shock history of the Bencubbin meteorite: A nitrogen, noble gas, and Ar-Ar investigation of silicates, metal and fluid inclusions. *Geochimica et Cosmochimica Acta* 74:6636–6653.

Maurer P., Eberhardt P., Geiss J., Grögler N., Stettler A., Brown G. M., Peckett A., and Krähenbühl U. 1978. Pre-Imbrian craters and basins: Ages, compositions and excavation depths of Apollo 16 breccias. *Geochimica et Cosmochimica Acta* 42:1687–1720.

McCallum I. S., Domeneghetti M. C., Schwartz J. M., Mullen E. K., Zema M., Cámara F., McCammon C., and Ganguly J. 2006. Cooling history of lunar Mg-suite gabbronorite 76255, troctolite 76535 and Stillwater pyroxenite SC-936: The record in exsolution and ordering in pyroxenes. *Geochimica et Cosmochimica Acta* 70:6068–6078.

McGee J. J., Bence A. E., Eichhorn G., and Schäffer O. A. 1978. Feldspathic granulite 79215—Limitations on T-f$_{O2}$ conditions and time of metamorphism. Proceedings, 9th Lunar and Planetary Science Conference. pp. 743–772.

Meyer J., Elkins-Tanton L., and Wisdom J. 2010. Coupled thermal–orbital evolution of the early Moon. *Icarus* 208:1–10.

Milton D. J. 1968. Miscellaneous geological investigations. In *Map 1-546, scale:1,000,000*. Washington, D.C.: U.S. Geological Survey.

Nakamura N., Masuda A., Tanaka T., and Kurasawa H. 1973. Chemical compositions and rare-earth features of four Apollo 16 samples. Proceedings, 4th Lunar Science Conference. pp. 1407–1414.

Nemchin A. A., Pidgeon R. T., Whitehouse M. J., Vaughan J. P., and Meyer C. 2008. SIMS U-Pb study of zircon from Apollo 14 and 17 breccias: Implications for the evolution of lunar KREEP. *Geochimica et Cosmochimica Acta* 72:668–689.

Nemchin A., Timms N., Pidgeon R., Geisler T., Reddy S., and Meyer C. 2009a. Timing of crystallization of the lunar magma ocean constrained by the oldest zircon. *Nature Geoscience* 2:133–136.

Nemchin A. A., Pidgeon R. T., Healy D., Grange M. L., Whitehouse M. J., and Vaughan J. 2009b. The comparative behavior of apatite-zircon U-Pb systems in Apollo 14 breccias: Implications for the thermal history of the Fra Mauro Formation. *Meteoritics & Planetary Science* 38:1717–1734.

Nisbet E. G. and Sleep N. H. 2001. The habitat and nature of early life. *Nature* 409:1083–1091.

Norman M. D. 2009. The lunar cataclysm: Reality or "mythconception"? *Elements* 1:23–28.

Norman M. D., Borg L. E., Nyquist L. E., and Bogard D. D. 2003. Chronology, geochemistry, and petrology of a ferroan noritic anorthosite clast from Descartes breccia 67215: Clues to the age, origin, structure, and impact history of the lunar crust. *Meteoritics & Planetary Science* 38:645–661.

Norman M. D., Duncan R. A., and Huard J. J. 2006. Identifying impact events within the lunar cataclysm from ^{40}Ar–^{39}Ar ages and compositions of Apollo 16 impact melt rocks. *Geochimica et Cosmochimica Acta* 70:6032–6049.

Norman M. D., Shih C.-Y., Nyquist L. E., Bogard D. D., and Taylor L. A. 2007. Early impacts on the Moon: Crystallization ages of Apollo 16 melt breccias (abstract #1991). 38th Lunar and Planetary Science Conference. CD-ROM.

Norman M. D., Duncan R. A., and Huard J. J. 2010. Imbrium provenance for the Apollo 16 Descartes terrain: Argon ages and geochemistry of lunar breccias 67016 and 67455. *Geochimica et Cosmochimica Acta* 74:763–783.

Nyquist L. E. and Wiesmann H. 1981. A 4. 2 AE whole rock Rb-Sr age for the Descartes Mountains. In *Workshop on Apollo 16*, edited by James O. B. and Hörz F. LPI Technical Report 81-01. Houston, Texas: Lunar and Planetary Institute. pp. 101–103.

Nyquist L. E., Reimold W. U., Bogard D. D., Wooden J. L., Bansal B. M., Wiesmann H., and Shih C.-Y. 1981. A comparative Rb-Sr, Sm-Nd and K-Ar study of shocked norite 78236: Evidence of slow cooling in the lunar crust? Proceedings, 12th Lunar and Planetary Science Conference. pp. 67–97.

Nyquist L. E., Shih C-Y., and Reese Y. D. 2008. Sm-Nd for norite 78236 and eucrite Y980318/433: Implications for planetary and solar system processes (abstract #1437). 39th Lunar and Planetary Science Conference. CD-ROM.

Nyquist L. E., Shih C.-Y., and Reese Y. D. 2012. Redetermination of the Sm-Nd age and initial epsilon-Nd of lunar troctolite 76535: Implications for lunar crustal development (abstract #2416). 43rd Lunar and Planetary Science Conference. CD-ROM.

Oberli F., Huneke J. C., McCulloch M. T., Papanastassiou D. A., and Wasserburg G. J. 1979. Isotopic constraints for the early evolution of the moon. *Meteoritics* 14:502–503.

Papanastassiou D. A. and Wasserburg G. J. 1976. Rb-Sr age of troctollite 76535. Proceedings, 7th Lunar Science Conference. pp. 2035–2054.

Petro N. E. and Pieters C. M. 2006. Modeling the provenance of the Apollo 16 regolith. *Journal of Geophysical Research* 111. doi:10.1029/2005JE002559

Pidgeon R. T., Nemchin A. A., van Bronswijk W., Geisler T., Meyer C., Compston W., and Williams I. 2007. Complex history of a zircon aggregate from lunar breccia 73235. *Geochimica et Cosmochimica Acta* 71:1370–1381.

Premo W. R. and Tatsumoto M. 1991. U-Th-Pb Isotopic systematics of lunar norite 78235 (abstract). 21st Lunar and Planetary Science Conference. p. 89.

Premo W. R. and Tatsumoto M. 1992. U-Th-Pb, Rb-Sr, and Sm-Nd isotopic systematics of lunar troctolite cumulate 76535: Implications on the age and origin of this early lunar, deep-seated cumulate. Proceedings, 22nd Lunar and Planetary Science Conference. pp. 381–397.

Prettyman T. H., Hagerty J. J., Elphic R. C., Feldman W. C., Lawrence D. J., McKinney G. W., and Vaniman D. T. 2006. Elemental composition of the lunar surface: Analysis of gamma ray spectroscopy data from Lunar Prospector. *Journal of Geophysical Research* 111. doi:10.1029/2005JE002656.

Reimold W. U. and Nieber-Reimold J. N. 1984. The mineralogical, chemical and chronological characteristics of the crystalline Apollo 16 impact melt rocks. *Fortschritte der Mineralogie* 62:269–301.

Reimold W. U., Nyquist L. E., Bansal B. M., Wooden J. L., Shih C.–Y., Weismann H., and MacKinnon I. D. R. 1985. Isotope analysis of crystalline impact melt rocks from Apollo 16, Stations 11 and 13, North Ray crater. Proceedings, 15th Lunar and Planetary Science Conference. pp. 431–C448.

Renne P. R., Swisher C. C., Deino A. L., Karner D. B., Owens T. L., and DePaolo D. J. 1998. Intercalibration of standards, absolute ages and uncertainties in $^{40}Ar/^{39}Ar$ dating. *Chemical Geology* 145:117–152.

Rose H. J., Cuttitta F., Berman S., Carron M. K., Christian R. P., Dwornik E. J., Greenland L. P., and Ligon D. T. 1973. Compositional data for twenty-two Apollo 16 samples. Proceedings, 4th Lunar Science Conference. pp. 1149–1158.

Ryder G. 1982. Lunar anorthosite 60025, the petrogenesis of lunar anorthosites and the composition of the Moon. *Geochimica et Cosmochimica Acta* 46:1591–1601.

Ryder G. 1990. Lunar samples, lunar accretion and the early bombardment of the Moon. *EOS* 71:322–323.

Ryder G. 2003. Bombardment of the Hadean Earth: Wholesome or deleterious? *Astrobiology* 3:3–6.

Schaeffer O. A. and Husain L. 1973. Early lunar history: Ages of 2 to 4 mm soil fragments from the lunar highlands. Proceedings, 4th Lunar Science Conference. pp. 1847–1863.

Schaeffer O. A. and Husain L. 1974. Chronology of lunar basin formation. Proceedings, 5th Lunar Science Conference. pp. 1541–1555.

Schaeffer G. A. and Schaeffer O. A. 1977. Ar-39-Ar-40 ages of lunar rocks. Proceedings, 8th Lunar Science Conference. pp. 2253–2300.

Schaeffer O. A., Husain L., and Schaeffer G. A. 1976. Ages of highland rocks—The chronology of lunar basin formation revisited. Proceedings, 7th Lunar Science Conference. pp. 2067–2092.

Schwarz W. H. and Trieloff M. 2007. Intercalibration of $^{40}Ar–^{39}Ar$ age standards NL-25, HB3gr hornblende, GA1550, SB-3, HD-B1 biotite and BMus/2 muscovite. *Chemical Geology* 242:218–231.

Shearer C. K., Hess P. C., Wieczorek M. A., Pritchard M. E., Parmentier E. M., Borg L. E., Longhi J., Elkins-Tanton L. T., Neal C. R., Antonenko I., Canup R. M., Halliday A. N., Grove T. L., Hager B. H., Lee D.-C., and Wiechert U. 2006. Thermal and magmativ evolution of the Moon. The constitution and structure of the lunar interior. In *New views of the Moon*, edited by Jolliff B., Wieczorek M. A., Shearer C. K., and Neal C. R. Washington, D.C.: Mineralogical Society of America. pp. 365–518.

Shearer C. K., Burger P. V., Neal C., Sharp Z., Spivak-Birndorf L., Borg L., Fernandes V. A., Papike J. J., Karner J., Wadhwa M., Gaffney A., Shafer J., Geissman J., Atudorei N.-V., Herd C., Weiss B. P., and King P. 2010. Non-basaltic asteroidal melting during the earliest stages of solar system evolution. A view from Antarctic achondrites Graves Nunatak 06128 and 06129. *Geochimica et Cosmochimica Acta* 74:1172–1199.

Shoemaker E. M. 1983. Asteroid and comet bombardment of the earth. *Annual Review of Earth and Planetary Sciences* 11:461–494.

Shuster D. L., Balco G., Cassata W. S., Fernandes V. A., Garrick-Bethell I., and Weiss B. P. 2010. A record of impacts preserved in the lunar regolith. *Earth and Planetary Science Letters* 290:155–165.

Snyder G. A., Borg L. E., Nyquist L. E., and Taylor L. A. 2000. Chronology and isotopic constraints on lunar evolution. In *Origin of the Earth and Moon*, edited by Canup R. M. and Righter K. Tucson, Arizona: The University of Arizona Press. pp. 361–395.

Sokol A. K., Fernandes V. A., Schulz T., Bischoff A., Burgess R., Clayton R. N., Münker C., Nishiizumi K., Palme H., Schultz L., Weckwerth G., and Mezger K. 2008. Geochemistry, petrology and ages of the lunar meteorites Kalahari 008 and 009: New constraints on early lunar evolution. *Geochimica et Cosmochimica Acta* 72:4845–4873.

Spohn T., Konrad W., Breuer D., and Ziethe R. 2001. The longevity of lunar volcanism: Implications of thermal evolution calculations with 2D and 3D mantle convection models. *Icarus* 149:54–65.

Spudis P. D. 1984. Apollo 16 site geology and impact melts: Implications for the geologic history of the lunar highlands. Proceedings, 15th Lunar and Planetary Science Conference. pp. C95–C107.

Spudis P. D. and Ryder G. 1981. Apollo 17 impact melts and their relation to the Serenitatis Basin. In *Multi-ring basins: Formation and evolution*. Proceedings, 11th Lunar and Planetary Science Conference. New York: Pergamon Press. pp. 133–148.

Spudis P. D., Wilhelms D. E., and Robinson M. S. 2011. Sculptured hills: Implications for the relative age of Serenitatis, basin chronologies, and the cratering history of the Moon (abstract #1365). 42nd Lunar and Planetary Science Conference. CD-ROM.

Staudacher T., Dominik B., Jessberger E. K., and Kirsten T. 1978. Consortium breccia 73255: $^{40}Ar-^{39}Ar$ dating. Proceedings, 9th Lunar and Planetary Science Conference. pp. 1098–1100.

Steiger R. H. and Jäger E. 1977. Subcommission on geochronology: Convention of the use of decay constants in geo- and cosmochronology. *Earth and Planetary Science Letters* 36:359–362.

Stöffler D. and Grieve R. 2007. Impactites. In *Metamorphic rocks: A classification and glossary of terms*, edited by Fettes D. and Demonds J. Cambridge: Cambridge University Press. pp. 82–91.

Stöffler D., Bischoff A., Borchardt R., Burghele A., Deutsch A., Jessberger E. K., Ostertag R., Palme H., Spettel B., Reimold W. U., Wacker K., and Wänke H. 1985. Composition and evolution of the lunar crust in the Descartes highlands, Apollo 16. Proceedings, 15th Lunar and Planetary Science Conference. pp. C449–C506.

Stöffler D., Ryder G., Ivanov B., Artemieva N. A., Cintala M. J., and Grieve R. A. F. 2006. Cratering history and lunar chronology. In *New views of the Moon*, edited by Jolliff B., Wieczorek M. A., Shearer C. K., and Neal C. R. Washington, D.C.: Mineralogical Society of America. pp. 519–596.

Swindle T. D., Isachsen C. E., Weirich J. R., and Kring D. A. 2009. ^{40}Ar–^{39}Ar ages of H-chondrite impact melt breccias. *Meteoritics & Planetary Science* 44:747–762.

Takeda H., Yamaguchi A., Bogard D. D., Karouji Y., Ebihara M., Ohtake M., Saiki K., and Arai T. 2006. Magnesian anorthosites and a deep crustal rock from the farside crust of the Moon. *Earth and Planetary Science Letters* 247:171–184.

Tera F., Papanastassiou D. A., and Wasserburg G. J. 1974. Isotopic evidence for a terminal lunar cataclysm. *Earth and Planetary Science Letters* 22:1–21.

Trieloff M., Jessberger E. K., and Oehm J. 1989. Ar-Ar ages of LL chondrites. *Meteoritics* 24:332.

Trieloff M., Kunz J., and Jessburger E. K. 1994. High-resolution Ar-40/Ar-39 dating of K-rich chondritic inclusions. *Meteoritics* 29:541–542.

Turner G. 1971. ^{40}Ar-^{39}Ar dating: The optimization of irradiation parameters. *Earth and Planetary Science Letters* 10:227–234.

Turner G. and Cadogan P. H. 1975. The history of lunar bombardment inferred from ^{40}Ar-^{39}Ar dating of highland rocks. Proceedings, 5th Lunar Science Conference. pp. 1509–1538.

Turner G., Huneke J. C., Podosek F. A., and Wasserburg G. J. 1971. ^{40}Ar-^{39}Ar ages and cosmic ray exposure ages of Apollo 14 samples. *Earth and Planetary Science Letters* 12:19–35.

Turner G., Cadogan P. H., and Yonge C. J. 1973. Argon selenochronology. Proceedings, 4th Lunar and Planetary Science Conference. pp. 1889–1914.

Turner G., Knott S. F., Ash R. D., and Gilmour J. D. 1997. Ar-Ar chronology of the Martian meteorite ALH 84001: Evidence for the timing of the early bombardment of Mars. *Geochimica et Cosmochimica Acta* 61:3835–3850.

Ulrich G. E. 1973. A geologic model for North Ray crater and stratigraphic implications for the Descartes region. Proceedings, 4th Lunar and Planetary Science Conference. pp. 27–39.

Vogel N. and Renne P. R. 2008. ^{40}Ar–^{39}Ar dating of plagioclase grain size separates from silicate inclusions in IAB iron meteorites and implications for the thermochronological evolution of the IAB parent body. *Geochimica et Cosmochimica Acta* 72:1231–1255.

Walker D., Longhi J., and Hays J. F. 1973. Petrology of Apollo 16 metaigneous rocks. Proceedings, 4th Lunar and Planetary Science Conference. pp. 752–754.

Wänke H., Palme H., Kruse H., Baddenhausen H., Cendales M., Dreibus G., Hofmeister H., Jagoutz E., Palme C., Spettel B., and Thacker R. 1976. Chemistry of lunar highland rocks: A refined evaluation of the composition of the primary matter. Proceedings, 7th Lunar Science Conference. pp. 3479–3499.

Wänke H., Baddenhausen H., Blum K., Cendales M., Dreibus G., Hofmeister H., Kruse H., Jagoutz E., Palme C., Spettel B., Thacker R., and Vilcsek E. 1977. On the chemistry of lunar samples and achondrites. Primary matter in the lunar highlands: A re-evaluation. Proceedings, 8th Lunar Science Conference. pp. 2191–2213.

Warren P. H. 2003. Lunar prospector data imply an age of 4.1 Ga for the Nectaris Basin, and other problems with the lunar "cataclysm" hypothesis (abstract #4129). 3rd International Conference on Large Meteorite Impacts, Nördlingen, Germany.

Wieczorek M. A. and Phillips R. J. 1999. Lunar multiring basins and the cratering process. *Icarus* 139: 246–259.

Wieczorek M. A., Jolliff B. L., Khan A., Pritchard M. E., Weiss B. P., Williams J. G., Hood L. L., Righter K., Neal C. R., Shearer C. K., McCallum I. S., Tompkins S., Hawke B. R., Peterson C., Gillis J. J., and Bussey B. 2006. The constitution and structure of the lunar interior. In *New views of the Moon*, edited by Jolliff B., Wieczorek M. A., Shearer C. K., and Neal C. R. Washington, D.C.: Mineralogical Society of America. pp. 222–364.

Wijbrans J. R. 1985. Geochronology of metamorphic terrains by the ^{40}Ar/^{39}Ar age spectrum method. PhD. thesis, Australian National University, Canberra.

Wilhelms D. E. 1987. *The geologic history of the Moon*. U.S. Geological Survey Professional Paper 1348. Washington, D.C.: U.S. Geological Survey. 302 p.

Wilhelms D. R. 1992. Last chance at the Taurus-Littrow. In *Workshop on geology of the Apollo 17 landing site*. LPI Technical Report 92-09. Houston, Texas: Lunar Science Institute. pp. 61–63.

Wilhelms D. E. and McCauley J. F. 1971. Geologic map of the near side of the Moon. In *USGS Map I-703, scale 1:5,000,000*. Washington, D.C.: U.S. Geological Survey.

Wilshire H. G. 1974. Provenance of Terra Breccias (abstract). 5th Lunar Science Conference. p. 846

Winzer S. R., Nava D. F., Lum R. K. L., Schuhmann S., Schuhmann P., and Philpotts J. A. 1975. Origin of 78235, a lunar norite cumulate. Proceedings, 6th Lunar Science Conference. pp. 1219–1229.

Wolfe E. W., Bailey N. G., Lucchitta B. K., Muehlberger W. R., Scott D. H., Sutton R. L., and Wilshire H. G. 1981. *The geologic investigation of the Taurus-Littrow Valley, Apollo 17 landing site*. U.S. Geological Survey Professional Paper 1080. Washington, D.C.: U.S. Geological Survey. 190 p.

Zellner N. E. B., Delano J. W., Swindle T. D., Barra F., Olsen E., and Whittet D. C. B. 2006. Did a transient increase in the impact flux occur 800 Ma ago? (abstract #1745). 37th Lunar and Planetary Science Conference. CD-ROM.

SUPPORTING INFORMATION

Additional Supporting Information may be found in the online version of this article:

Appendix S1: Thin sections of the Apollo 16 Station 13 soil samples investigated in this study are displayed by transmitted light micrographs. Micrographs with plane and crossed polarizers are combined to illustrate the petrographic and shock metamorphic features of the samples. Note that all mineral show unusual interference colours because the available thin sections are substantially thicker than common 25 μm.

Appendix S2: Electron microprobe analyses.

Appendix S3: ^{40}Ar/^{39}Ar data.